# *Chapter 2*
# *THE DEVIATION OPERATOR*

We really do not want to abandon the separable form unless there is a strong reason to do so, because it gives us the advantage of working either in midpoint or offset space, independently. So we ask ourselves the following question: can we build a theory for the Sep(Y,H) operator such that it will relax the zero-dip and zero-offset assumptions, at least to a certain degree of accuracy? In this chapter we will look for an answer to this question.

## *2-1 Fundamental Concepts*

Common sense suggests that the answer must be present in the discrepancy between the operators DSR(Y,H) and Sep(Y,H). Therefore, we are motivated to make the following formal definition:

$$Dev(Y,H) = DSR(Y,H) - Sep(Y,H) \qquad (2\text{-}1)$$

The operator Dev(Y,H) describes the deviation of conventional processing from the exact theory of wave extrapolation. Substituting (1-31) and (1-40) into (2-1) we obtain the full expression for this operator

$$\mathrm{Dev}(Y,H) = \left[ 1 - \left( Y + H \right)^2 \right]^{1/2} + \left[ 1 - \left( Y - H \right)^2 \right]^{1/2} \qquad (2\text{-}2)$$

$$- 2 \left( 1 - Y^2 \right)^{1/2} - 2 \left( 1 - H^2 \right)^{1/2} + 2$$

(2-2) looks rather formidable. We would like to obtain a simpler expression for it; thus, with a little courage, we make an approximation. To second order in Y, i.e. $1 > H \gg Y$, we expand the DSR and Sep operators using the square root expansions provided in Appendix A. With (A-1), (1-40) is expanded as follows:

$$\mathrm{Sep}(Y,H) = 2 \left( 1 - Y^2 \right)^{1/2} + 2 \left( 1 - H^2 \right)^{1/2} - 2$$

$$\simeq 2 \left( 1 - \frac{Y^2}{2} \right) + 2 \left( 1 - H^2 \right)^{1/2} - 2$$

Simplifying,

$$\mathrm{Sep}(Y,H) \simeq - Y^2 + 2 \left( 1 - H^2 \right)^{1/2} \qquad (2\text{-}3)$$

Similarly, using (A-2), DSR(Y,H) is expanded as follows:

$$DSR(Y,H) = \left[ 1 - \left( Y + H \right)^2 \right]^{1/2} + \left[ 1 - \left( Y - H \right)^2 \right]^{1/2}$$

$$\simeq \left( 1 - H^2 \right)^{1/2} \left[ 1 - \frac{H\,Y}{1 - H^2} - \frac{Y^2}{2\left( 1 - H^2 \right)^2} \right]$$

$$+ \left( 1 - H^2 \right)^{1/2} \left[ 1 + \frac{H\,Y}{1 - H^2} - \frac{Y^2}{2\left( 1 - H^2 \right)^2} \right]$$

Simplifying, we have the final expression

$$DSR(Y,H) \simeq 2 \left( 1 - H^2 \right)^{1/2} - \left( 1 - H^2 \right)^{-3/2} Y^2 \qquad (2\text{-}4)$$

We substitute (2-3) and (2-4) into (2-1), and obtain the approximate form for the deviation operator

$$Dev(Y,H) \simeq \left[ 1 - \left( 1 - H^2 \right)^{-3/2} \right] Y^2 \qquad (2\text{-}5)$$

Expanding (2-5) to second order in H yields a simpler but coarser

approximation in H

$$Dev(Y,H) \approx -\frac{3}{2} H^2 Y^2 \qquad (2\text{-}6)$$

A closer look at these approximations will reveal the fact that, in both, H and Y are coupled. This defeats the whole point of improving the separable form Sep(Y,H) of conventional processing. Specifically, we would like to come up with a procedure which, together with moveout correction, maps common offset sections onto zero offset more accurately. The only possibility of utilizing the deviation term is to replace H by an estimate of $\hat{H}$ such that $\hat{H}$ does not depend on the spatial frequency $k_h$ which couples adjoining offsets. We therefore redefine the deviation operator by substituting $\hat{H}$ for H in (2-1):

$$Dev(Y,\hat{H}) = DSR(Y,\hat{H}) - Sep(Y,\hat{H}) \qquad (2\text{-}7)$$

The approximate forms (2-5) and (2-6) are now

$$Dev(Y,\hat{H}) \approx \left[ 1 - \left( 1 - \hat{H}^2 \right)^{-3/2} \right] Y^2 \qquad (2\text{-}8)$$

and

$$Dev(Y,\hat{H}) = -\frac{3}{2} \hat{H}^2 Y^2 \qquad (2\text{-}9)$$

These approximations can now be implemented in midpoint space.

How do we estimate $\hat{H}$ ? To answer this question we recall the Fourier solution exp ( $-i\omega t + ik_h h$ ) , upon which H is defined. Staying at a constant phase implies

$$- \omega \, dt + k_h \, dh = 0$$

or

$$\frac{dt}{dh} = \frac{k_h}{\omega} \qquad (2\text{-}10)$$

For a constant velocity medium, Equation (B-10b) of Appendix B reads

$$\left[ h^2 + z^2 \right]^{1/2} = \frac{v \, t}{2} \qquad (2\text{-}11)$$

From which we may compute the stepout dt/dh,

$$4 \left[ h^2 + z^2 \right]^{1/2} = v^2 \, t^2$$

$$4 \, h \, dh = v^2 \, t \, dt$$

Finally,

$$\frac{dt}{dh} = \frac{4\ h}{v^2\ t} \qquad (2\text{-}12)$$

Substituting (2-12) into (2-10) and recalling the definition for $H = v\ k_h\ /\ 2\ \omega$, we have the estimate

$$\hat{H} = \frac{v}{2}\frac{k_h}{\omega}$$

$$= \frac{v}{2}\frac{dt}{dh}$$

$$\hat{H} = \frac{2\ h}{v\ t} \qquad (2\text{-}13a)$$

Equation (2-13a) defines H in terms of surface offset and two-way traveltime. This supports our intuition that we expect to see different stepouts dt/dh at different offsets and times. The moveout equation (2-11) is also valid for stratified earth if we take v to be the RMS velocity down to depth z, in which case

$$\hat{H} = \frac{2\ h}{v_{RMS}\ t} \qquad (2\text{-}13b)$$

Notice also that (2-13) is in the form that we wish, i.e. the offset value enters as a parameter into the deviation operator. Another estimate for $\hat{H}$ could be made to improve (2-13) by including a regional dip factor. It is well known that the RMS velocity estimated from CMP gathers has a dip dependency

$$v_{RMS} = \frac{v}{\cos(\theta)} \tag{2-14}$$

where $\theta$ is regional dip and v is true medium velocity.

In more general cases $\hat{H}$ could be determined by ray tracing from theoretical velocity models or perhaps estimated by smoothing data. As it will be seen from model experiments, the main point to keep in mind is that great accuracy is not required.

Our estimate for $\hat{H}$ makes the coefficients of the approximate $Dev(Y,\hat{H})$ operators (2-8) and (2-9) scalar-like quantities. The computational cost of these two approximations is the same, but their accuracies differ. Therefore, we are inclined to choose (2-8), which is a better approximation in H. Figure 2-1 shows the impulse responses of the exact and approximate forms of $Dev(Y,\hat{H})$. The following transfer function

$$e^{-i \frac{\omega}{v} Dev(k_y,\omega,\hat{H})\, z} \tag{2-15}$$

was computed and inverse Fourier transformed over $k_y$ and $\omega$. In (2-15) the full expression for $Dev(k_y,\omega,\hat{H})$ in the case of (2-7) is

$$Dev(k_y,\omega,\hat{H}) = \left[ 1 - \left( \frac{v\ k_y}{2\ \omega} + \hat{H} \right)^2 \right]^{1/2} + \left[ 1 - \left( \frac{v\ k_y}{2\ \omega} - \hat{H} \right)^2 \right]^{1/2} \quad (2\text{-}16a)$$

$$- 2 \left[ 1 - \left( \frac{v\ k_y}{2\ \omega} \right)^2 \right]^{1/2} - 2 \left[ 1 - \hat{H}^2 \right]^{1/2} + 2$$

In the case of (2-8), it is

$$Dev(k_y,\omega,\hat{H}) = \left[ 1 - \left( 1 - \hat{H}^2 \right)^{-3/2} \right] \left( \frac{v\ k_y}{2\ \omega} \right)^2 \quad (2\text{-}16b)$$

and in case of (2-9)

$$Dev(k_y,\omega,\hat{H}) = - \frac{3}{2} \hat{H}^2 \left( \frac{v\ k_y}{2\ \omega} \right)^2 \quad (2\text{-}16c)$$

where

$$\hat{H} = \frac{h\ /\ z}{\left( 1 + h^2\ /\ z^2 \right)^{1/2}} \quad (2\text{-}17)$$

which is equivalent to (2-13a) by way of (2-11).

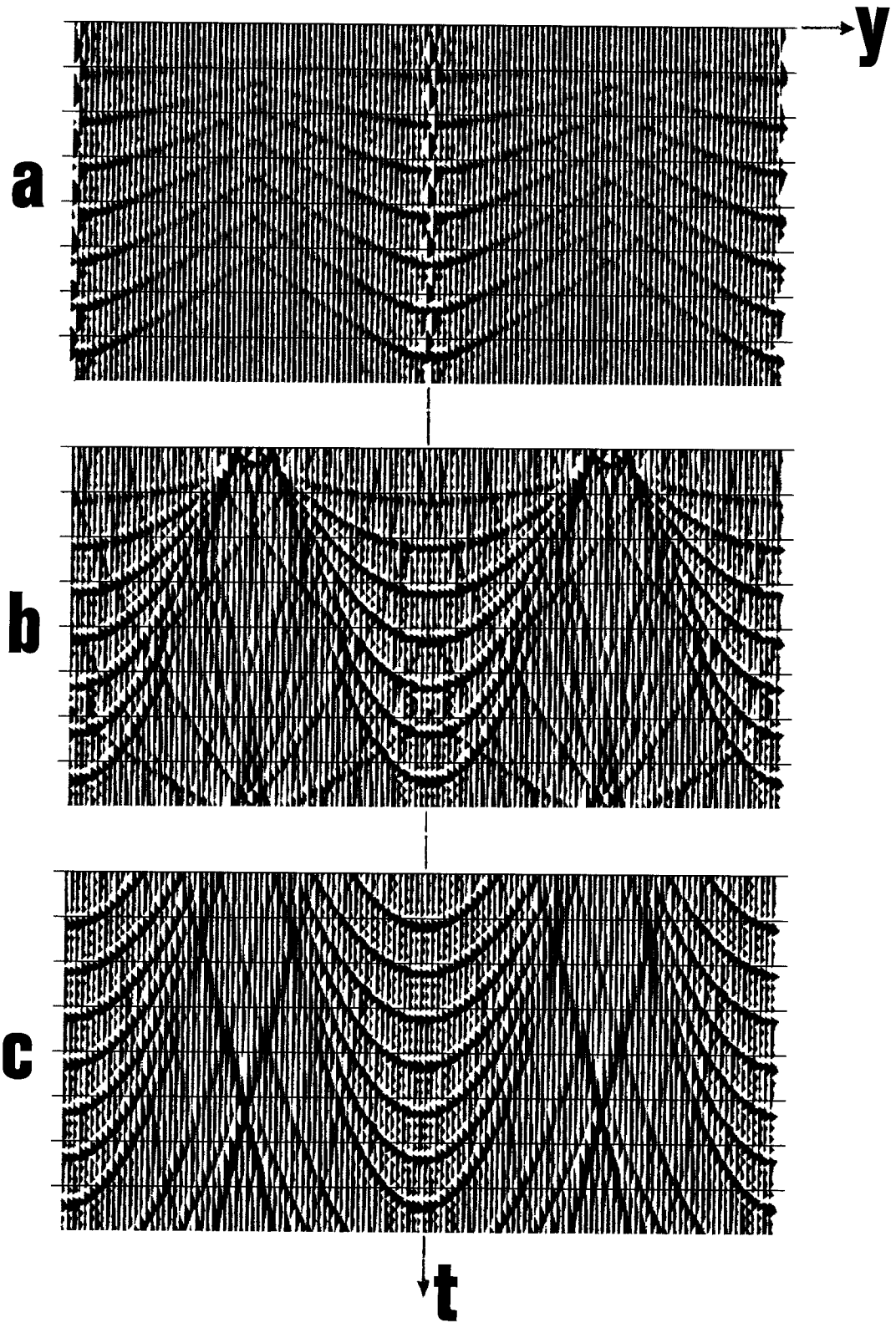


FIG. 2-1. Impulse response of the deviation operator to point scatterers buried at z = 200-1400 m at intervals of 200 m. (a) Exact form of Dev(Y,H) given by (2-16a) is used in (2-15), (b) Second order approximation in Y given by (2-16b) is used in (2-15), and (c) Second order approximation both in Y and H given by (2-16c) is used in (2-15).

The discretization intervals in Figure 2-1 are $\Delta h = \Delta y = \Delta z = 25m$, and the medium velocity is 3000 m/sec and h = 400 m. Each figure is actually a superposition of seven (y,t)-planes at indicated z-levels. Physical interpretation is as follows: Given a common offset section with point-like responses in (y,t)-space, the operator $Dev(Y,\hat{H})$ maps it onto zero offset along the trajectories seen in Figure 2-1. The loci of the trajectories for (2-8) and (2-9) were determined by stationary phase approximation (Appendix B, Section B-4). Each trajectory in Figure 2-1b,c is a parabola. An important conclusion that we can draw from the impulse responses is that we are certainly better off by choosing (2-8) for implementation. Its mapping trajectories are closer to the exact one (a).

In the next section, we will develop an algorithm which we hope will remove the deficiency of the Sep(Y,H) operator for wide offsets. Adding $Dev(Y,\hat{H})$ onto Sep(Y,H) we have

$$NewSep(Y,H) = Sep(Y,H) + Dev(Y,\hat{H}) \qquad (2\text{-}18)$$

Recalling that Sep(Y,H) represents conventional processing, it is proper to say that NewSep(Y,H) represents "improved" conventional processing. Actually, (2-18) can be directly obtained from the definition of Sep(Y,H) given by (1-39). We derived (1-40) by setting $H_o = Y_o = 0$ in (1-39). Now, letting $H_o = \hat{H}$ , $Y_o = 0$ , we have

$$Sep(Y,H;H_o=\hat{H},Y_o=0) = DSR(Y,\hat{H}) + DSR(0,H) - DSR(0,\hat{H}) \qquad (2\text{-}19a)$$

Rewriting (1-39),

$$Sep(Y,H;H_o=0,Y_o=0) = DSR(Y,0) + DSR(0,H) - DSR(0,0) \qquad (2\text{-}19b)$$

Now recall the definition for $Dev(Y,\hat{H})$ from (2-7):

$$Dev(Y,\hat{H}) = DSR(Y,\hat{H}) - Sep(Y,\hat{H})$$

$$Dev(Y,\hat{H}) = DSR(Y,\hat{H}) - \left[ DSR(Y,0) + DSR(0,\hat{H}) - DSR(0,0) \right] \qquad (2\text{-}19c)$$

Adding (2-19b) and (2-19c) and comparing the result with (2-19a),

$$Sep(Y,H;H_o=\hat{H},Y_o) = Sep(Y,H;H_o=0,Y_o=0) + Dev(Y,\hat{H})$$

Comparing with (2-18) we see that

$$NewSep(Y,H)=Sep(Y,H;H_o=\hat{H},Y_o=0) \qquad (2\text{-}20)$$

which implies that NewSep is the old Sep with a nonzero $H_o = \hat{H}$, which conventional processing takes as zero.

## *2-2 Pre-stack Partial Migration Equation*

We now describe the implementation of the approximate form (2-8) of the deviation operator. Combining (2-13a) and (1-30a), and incorporating the missing scalar $\omega$ / v , we have

$$k_z = -\frac{\omega}{v}\left\{1 - \left[1 - \left(\frac{2\,h}{v\,t}\right)^2\right]^{-3/2}\right\}\left(\frac{v\,k_y}{2\,\omega}\right)^2 \qquad (2\text{-}21)$$

Simplifying, we have the final expression

$$\omega\,k_z = -\frac{\tilde{v}}{4}\,k_y^2 \qquad (2\text{-}22)$$

where

$$\tilde{v} = v\left\{1 - \left[1 - \left(\frac{2\,h}{v\,t}\right)^2\right]^{-3/2}\right\} \qquad (2\text{-}23)$$

Notice that (2-22) is in the form of the retarded 15-degree approximation to the zero-offset migration equation (1-34). The difference between them is that the extrapolation velocity in (2-22) is not the medium velocity but the one defined by (2-23). Since this velocity is t-dependent, Equation (2-22) cannot be implemented in $\omega$-space. Assuming no lateral variation in velocity, it can be implemented in $(k_y,t)$ -space. As will be seen in model experiments, insensitivity to velocity

variation makes this process robust enough for us to in fact neglect any lateral variations in velocity. Initial implementation was actually done in the (y,t)-domain.

Referring to (2-23), $\tilde{v}$ is actually defined as a negative quantity since $\hat{H} \leq 1$ . Keeping this in mind, (2-22) yields the following partial differential equation:

$$P_{zt} = \frac{\tilde{v}}{4} P_{yy} \tag{2-24}$$

This is the ***pre-stack partial migration equation*** applied on a common offset section, which is not moveout corrected. $\tilde{v}$ is interpreted as the velocity of propagation adjusted for offset in the manner described by (2-23).

Equation (2-22) can also be used in the case of a stratified medium. It is convenient, however, to make the conversion

$$\tau = 2 \int_0^z \frac{dz}{v(z)} \tag{2-25}$$

which yields

$$P_{\tau t} = \frac{v^2}{8} \left\{ 1 - \left[ 1 - \left( \frac{2\,h}{v_{RMS}\,t} \right)^2 \right]^{-3/2} \right\} P_{yy} \tag{2-26}$$

Here, we substitute (2-13b) for $\hat{H}$ . Notice however that $v_{RMS}$ is really

a function of the two-way zero-offset traveltime. We therefore need to transform (2-26) to NMO coordinates defined as follows:

$$t' = t \left[ 1 - \left( \frac{2\,h}{v_{RMS}\,t} \right)^2 \right]^{1/2} \qquad (2\text{-}27a)$$

and

$$h' = h \qquad (2\text{-}27b)$$

We also have the principal of invariance

$$P(y,h,\tau,t) = P'(y,h',\tau,t') \qquad (2\text{-}28)$$

The critical partial differentiation is

$$\frac{\partial P}{\partial t} = \frac{\partial P'}{\partial t'} \frac{\partial t'}{\partial t} + \frac{\partial P'}{\partial h'} \frac{\partial h'}{\partial t} \qquad (2\text{-}29)$$

$\partial P' / \partial h'$ is negligible for moveout-corrected data. Using (2-27)

$$\frac{\partial t'}{\partial t} = \left[ 1 + \left( \frac{2\ h}{v_{RMS}\ t'} \right)^2 \right]^{1/2} \qquad (2\text{-}30)$$

Inverting (2-27a) and using (2-30) we obtain the moveout-corrected form of (2-26):

$$P_{\tau t'} = \frac{v^2}{8} \left\{ 1 - \left[ 1 + \left( \frac{2\ h}{v_{RMS}\ t'} \right)^2 \right]^{3/2} \right\} \left[ 1 + \left( \frac{2\ h}{v_{RMS}\ t'} \right)^2 \right]^{-1/2} P_{yy} \qquad (2\text{-}31)$$

The small offset approximation to (2-31) is

$$P_{\tau t'} = - \frac{v^2}{8} \frac{3}{2} \left( \frac{2\ h}{v_{RMS}\ t'} \right)^2 P_{yy} \qquad (2\text{-}32)$$

It is instructive to compare (2-32) with the pre-stack migration equation given by Claerbout (1976) in "Fundamentals of Geophysical Data Processing" [ page 253, Equation (11-3-19) ]. That equation in the present notation is

$$P_{\tau t'} = -\frac{v^2}{8} \left[ 1 + \left( \frac{2\ h}{v\ t'} \right)^2 \right] P_{yy} \qquad (2\text{-}33)$$

(2-33) has been derived for a constant velocity medium and is a 15-degree-type equation. The part that is equivalent to the pre-stack partial migration equation (2-32) has a missing factor of 3/2. This inconsistency is yet to be resolved. The fact is that (2-33) is based on the downward continuation of receivers, only, whereas the present result (2-32) is based on the double square root equation, which represents the downward continuation of both shots and receivers.

A final consideration is that the pre-NMO equation (2-24) has a pole at t=2h/v [ Equation (2-23) ], whereas the post-NMO equation (2-31) has a pole at t' = 0 . At first, the presence of the poles seems worrisome. However, we may stop the extrapolation at the poles for two reasons: (a) angles become so large that our equations cannot handle them properly, and (b) non-zero data for t < 2h/v would not fit a wave propagation model.

The 15-degree finite difference computational star described by Claerbout (1976) can be used to solve (2-24) and (2-31) numerically. Writing (2-24) in difference form,

$$\delta_z \delta_t P = -a \delta_{xx} P \qquad (2\text{-}34)$$

where $\delta$ is the difference operator and

$$a = \frac{|\tilde{v}| \Delta z \Delta t}{16 \Delta x^2} \qquad (2\text{-}35)$$

The t-outer algorithm (Claerbout, 1976) was used in the present analysis for two reasons: (a) less memory is required, and (b) more important, $\hat{H}$ is constant along the extrapolation path (Figure 2-2a). Notice that the

extrapolation coefficient "a" defined by (2-35) is a function of offset and traveltime via (2-23). Numerically, for stability reasons, we prefer "a" to be a global constant over the entire (z,t)-plane. This suggests that the number of z-steps will vary with time t. Solving (2-35) for $\Delta z$ , we determine the number of z-steps at a given time t. Figure 2-2b,c is a graph of the number of z-steps as a function of time for pre- and post-NMO equations. Notice that the number of z-steps increases rapidly near the pole. Figure 2-2 suggests that, we start with a small number of z-steps at the bottom of the (z,t)-frame, i.e. we use a very coarse extrapolation interval, which is unlike how we would proceed using a finite-difference migration scheme. As we go up the section in time, we extrapolate at much finer intervals as depicted in Figure 2-2a. This is a desirable property for an algorithm that operates mostly on wide offset angles (large h or small t), although it does necessitate an interpolation procedure to resample the (z,y)- or $(z,k_y)$-plane. In the next section, experiments on interpolation will be described.

## *2-3 Model Experiments*

We will test the performance of the pre-stack partial migration procedure, both before and after moveout correction. We also would like to determine some of its properties, such as sensitivity to velocity variation and offset value. An ideal testing model is point scatterers buried at various depths. Such a model would consist of a wide range of dips. Figure 2-3 shows common offset sections with h = 0 and h = 400 m over such an earth model.

Figure 2-4 illustrates different numerical techniques for the interpolation required during extrapolation in z. Although the nearest neighbor technique is the cheapest, it is obviously an undesirable choice. Because coarse interpolation creates artificial diffractors, thereby causing a noisy appearance. Linear interpolation could be considered as a possible means of interpolation in the production-oriented implementation of pre-stack partial migration. The four-point Lagrangian technique, which is a specialized form of Aitken's algorithm for

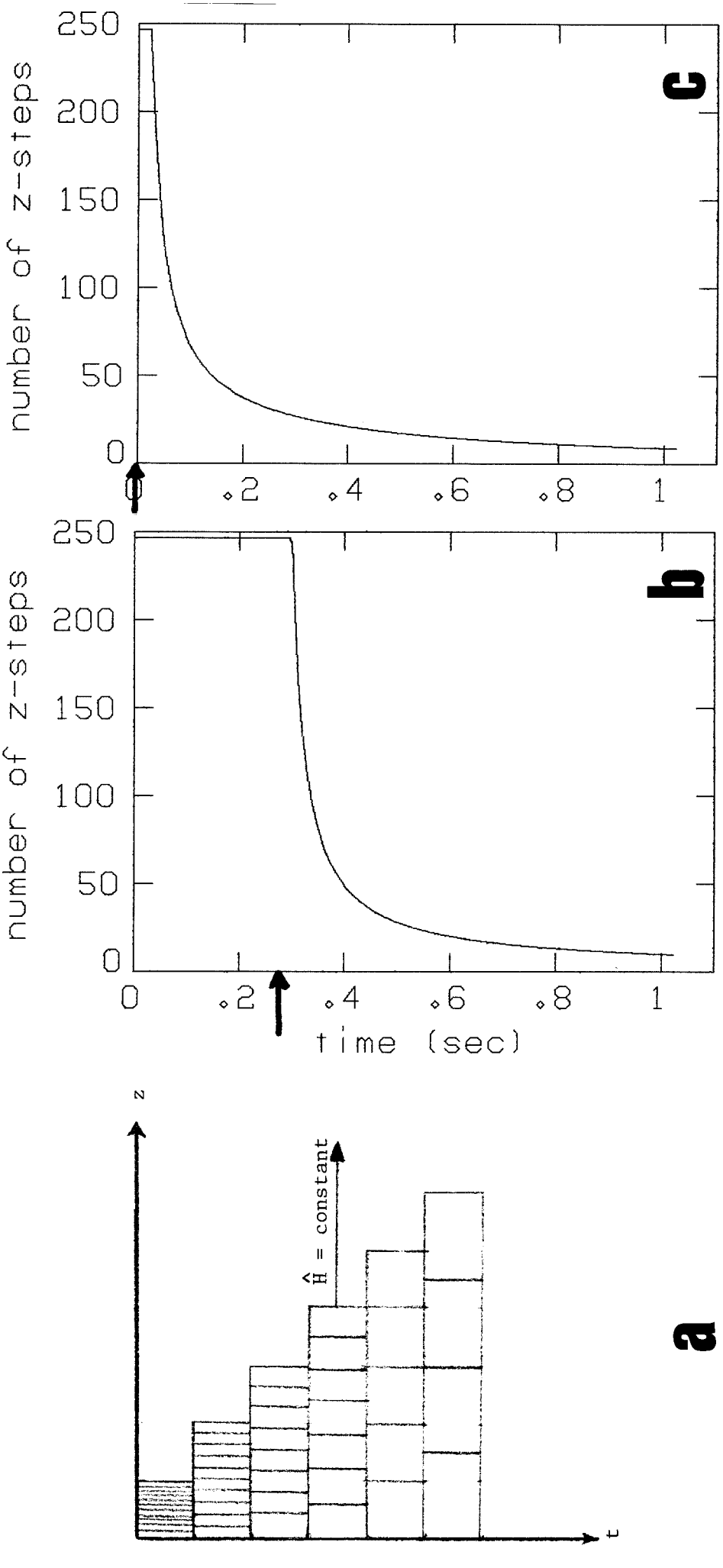


FIG. 2-2. Extrapolation and interpolation of wavefields with the pre-stack partial migration equation: (a) We start at the bottom of the (z,t) -plane and work our way up in t. Each cell represents a vector in y or $k_y$ . At each t-level, H is a fixed scalar. As we move upward in section, we interpolate between z-steps of level t to extrapolate the wavefield at level t-$\Delta$t . Notice that the number of z-steps increases as we go up the section as shown in (b) for the pre-NMO equation (2-24) and in (c) for the post-NMO equation (2-31). The poles are indicated by the arrows.

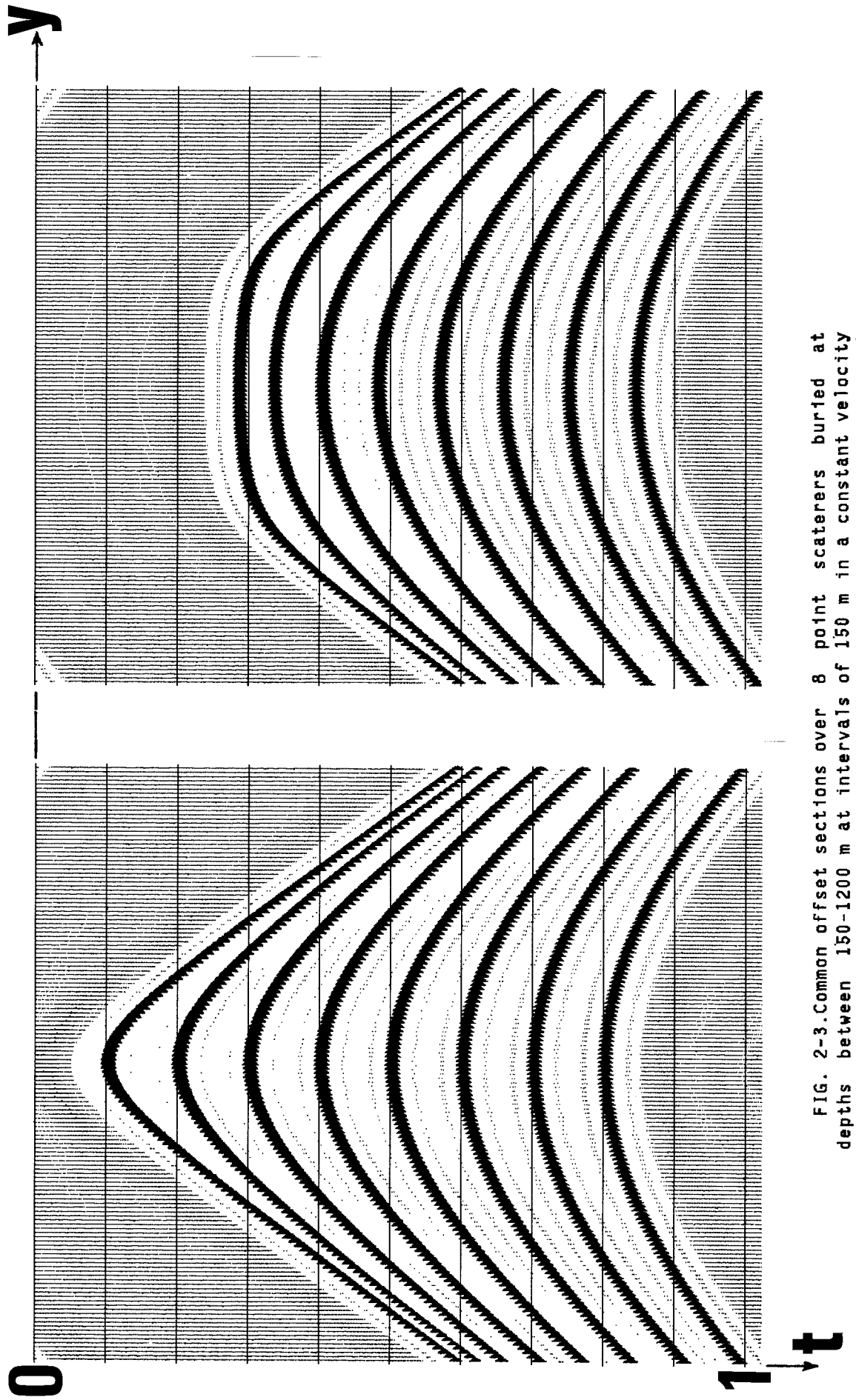


FIG. 2-3.Common offset sections over 8 point scaterers buried at depths between 150-1200 m at intervals of 150 m in a constant velocity medium (v = 3000 m/sec): (a) the zero-offset section (h = 0), and (b) common offset section with h = 400 m. Note the table-top appearance of the response of the shallow event on the far offset section. Sampling interval is 4 msec and midpoint spacing is 12.5 m. The bandwidth is 6,12 - 36,48 Hz. Amplitudes decay as $t^{-1/2}$.

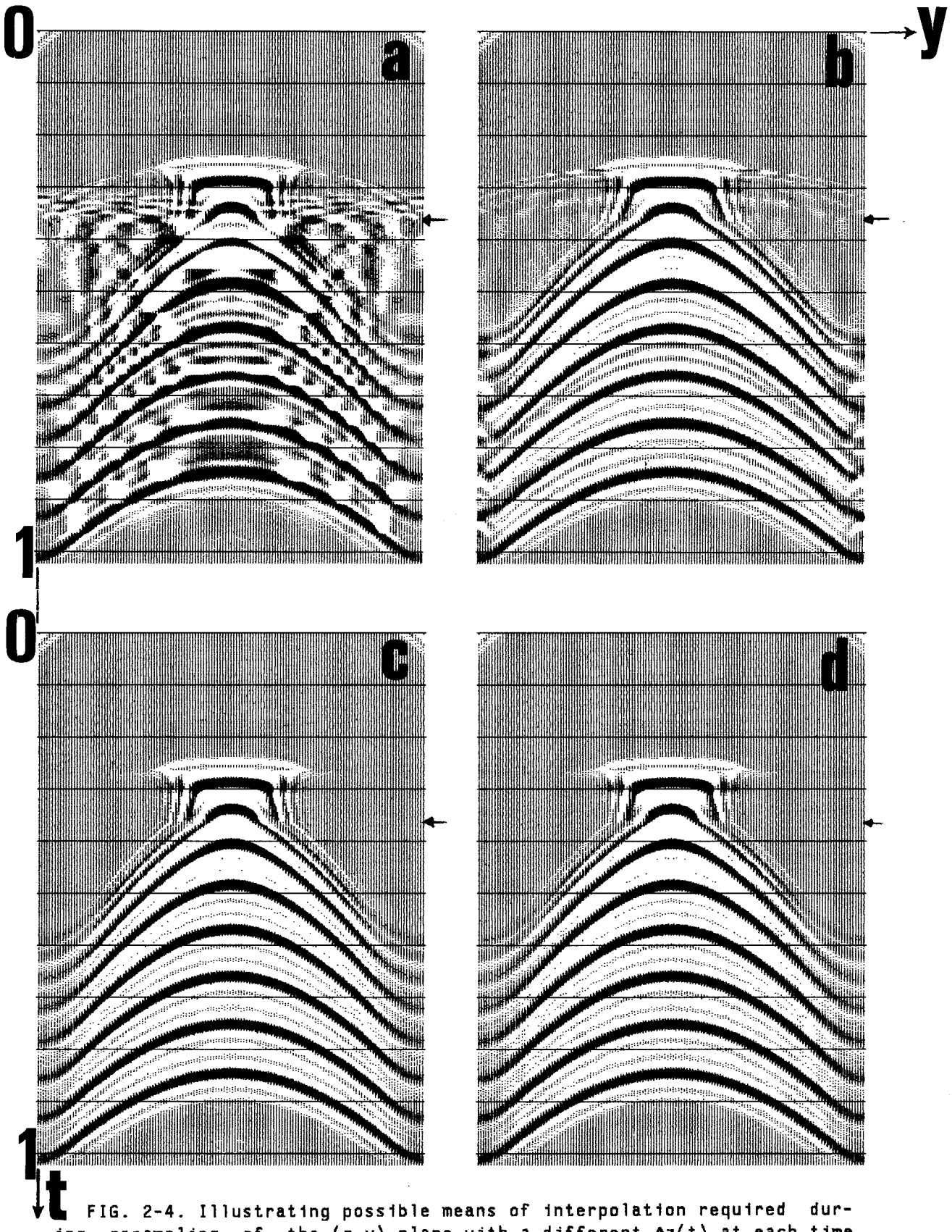


FIG. 2-4. Illustrating possible means of interpolation required during resampling of the (z,y)-plane with a different $\Delta z(t)$ at each time sample. (a) Nearest neighbor results in undesired numerical artifacts, (b) linear interpolation may be considered for production-oriented algorithms even though it has some undesirable features, as can be seen on the margins, (c) the four-point Lagrangian, and (d) cubic spline are the most desirable types of interpolation. Arrows indicate the time beyond which the number of z-steps is fixed due to limitation in data storage. This caused the under-processing of the data above the arrows.

interpolation (Conte, 1965), and the technique of cubic spline (L. Morley, personal comm.) perform equally well; the latter however is computationally more attractive. Remaining model tests and field data processing were done using the cubic spline technique for interpolation.

Figure 2-4 illustrates a problem of concern to us. Notice that near the pole there is actually a discontinuity. This is due to the limitation on the number of z-steps that can be handled by the computer. Theoretically, one needs to take an immense number of z-steps near the pole. If we make an attempt to allow more z-steps, we introduce dispersion, as shown in Figure 2-5a. If we take coarser z-steps, the resulting output is poorer (Figure 2-5b). As we near the pole, t approaches 2h/v. This implies extremely large offset angles, which are not accurately handled by our equation, and explains the anisotropic dispersion near the pole in Figure 2-5a. To better understand this problem, we should perhaps study the impulse response of our operator. Figure 2-6a is the common offset section that would be recorded over semi-elliptical reflecting horizons. Although such horizons are not realistic, we would still like to see what pre-stack partial migration will do to them. If this were a common offset section with h = 200 m, the zero-offset mapping would be as shown in Figure 2-6b. If it were treated as a common offset section with h = 400 m, the mapping would be as shown in Figure 2-6c. The impulse response as obtained via finite difference formulation is identical to the response computed by inverse Fourier transforming the transfer function (Figure 2-1b). The impulse response clearly demonstrates the role of the offset: the larger the offset and the shallower the event, the wider the range of midpoints involved in mapping to zero offset. We can also see the response near the pole that produces evanescent energy. The impulse response of the post-NMO operator is shown in Figure 2-7. Note its behavior is similar to that produced by the pre-NMO operator.

Figures 2-8 and 2-9 illustrate the comparative performance of the pre- and post-NMO differential equations. These and subsequent model studies were done in the $(k_y,t)$ -domain. The post-NMO operator is clearly superior to the pre-NMO operator. Again, as we near the pole $t' = 0$ , we observe the anisotropic dispersion. A proper test of the

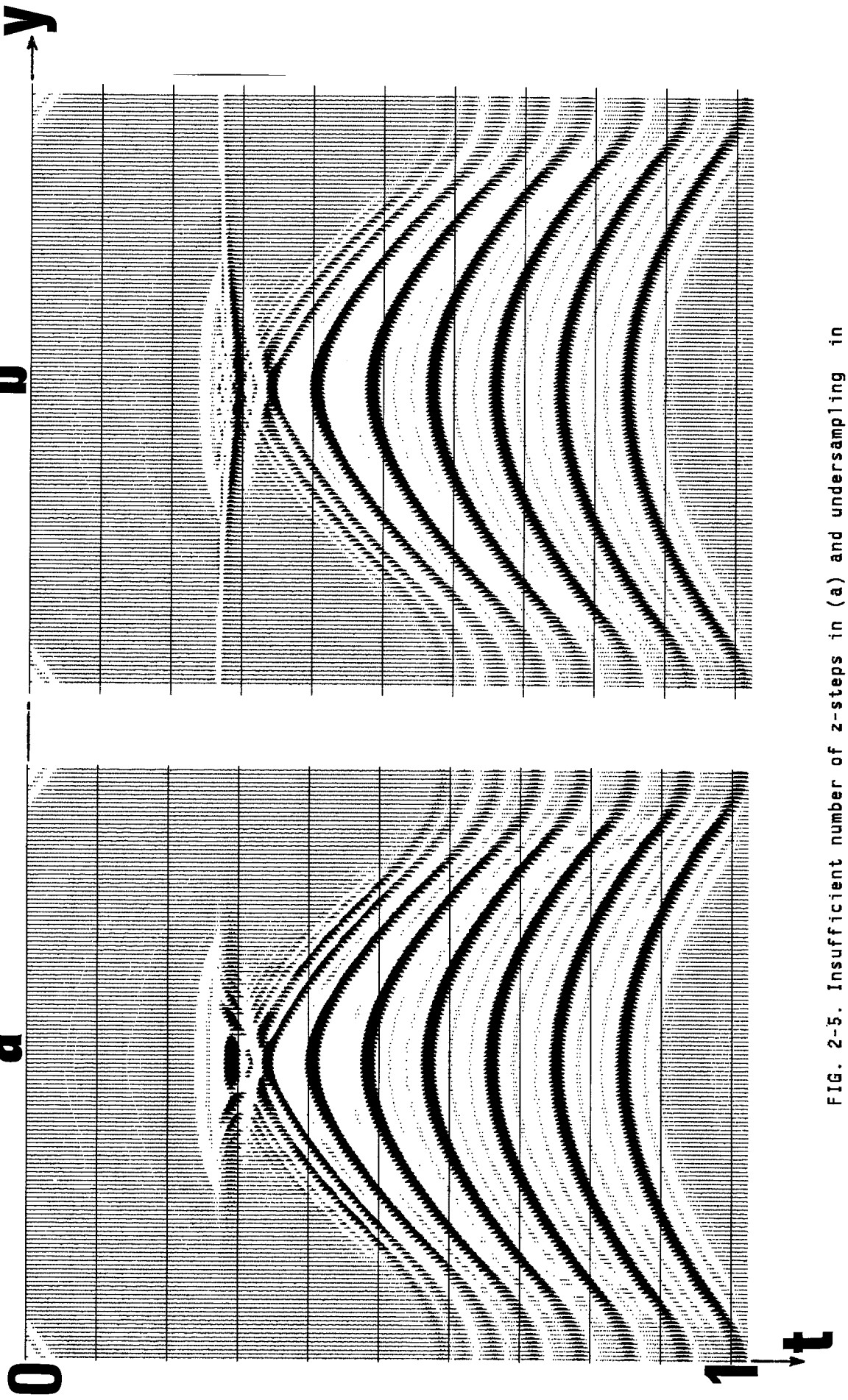


FIG. 2-5. Insufficient number of z-steps in (a) and undersampling in $\Delta z$ in (b) clearly show the incomplete mapping of the top event to zero offset. Dispersion near the top event is partly anisotropic, which is due to the limited accuracy of Equation (2-24) very near the pole at $t = 2h/v$.

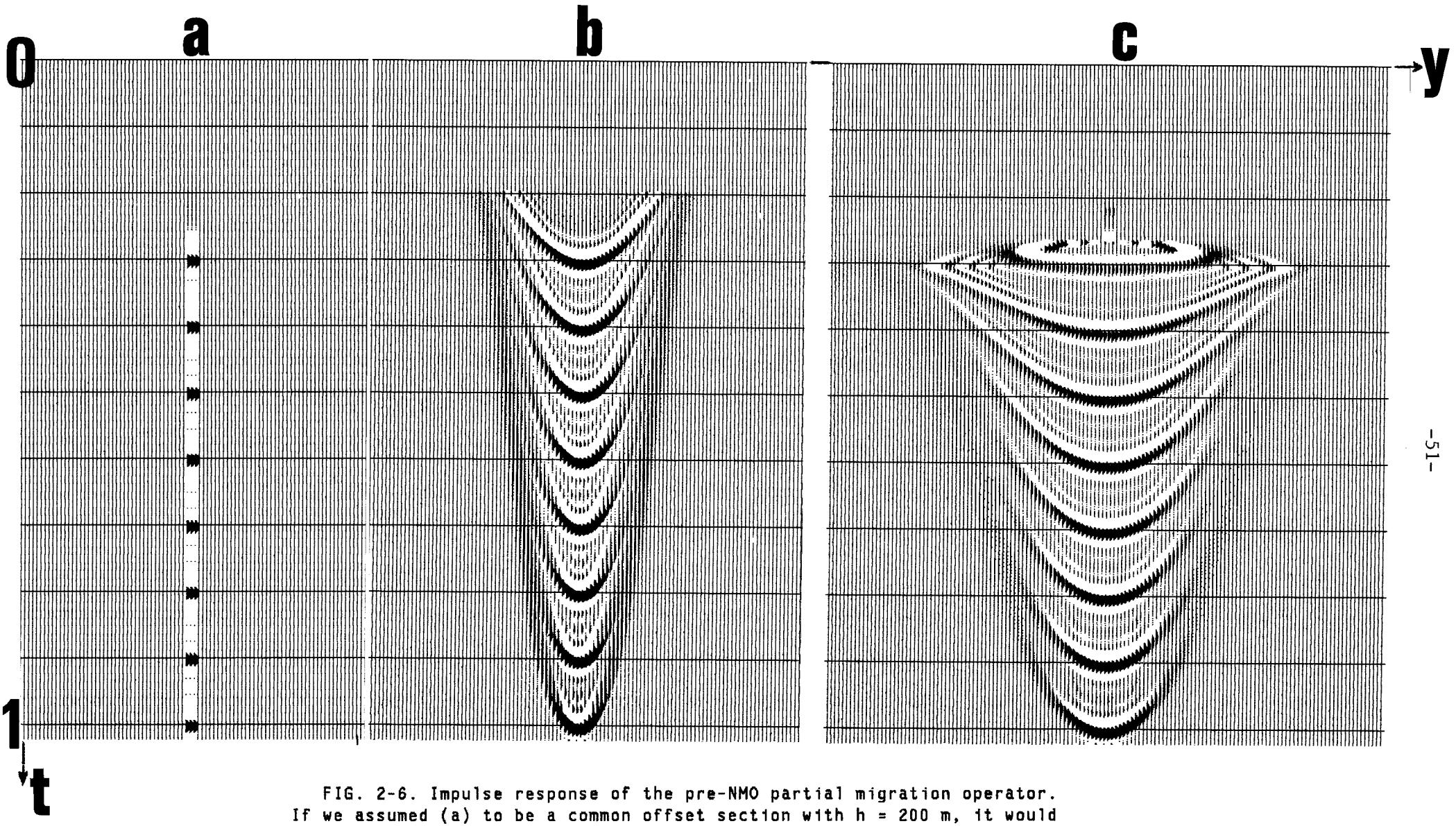


FIG. 2-6. Impulse response of the pre-NMO partial migration operator. If we assumed (a) to be a common offset section with h = 200 m, it would be mapped onto zero offset as shown in (b). If we assumed (a) to be a common offset section with h = 400 m, it would be mapped onto zero offset as shown in (c). We observe that the mapping involves a larger number of midpoints for large values of offset (h) and for shallower events (small t). Notice the anisotropic behavior near the pole in (c).

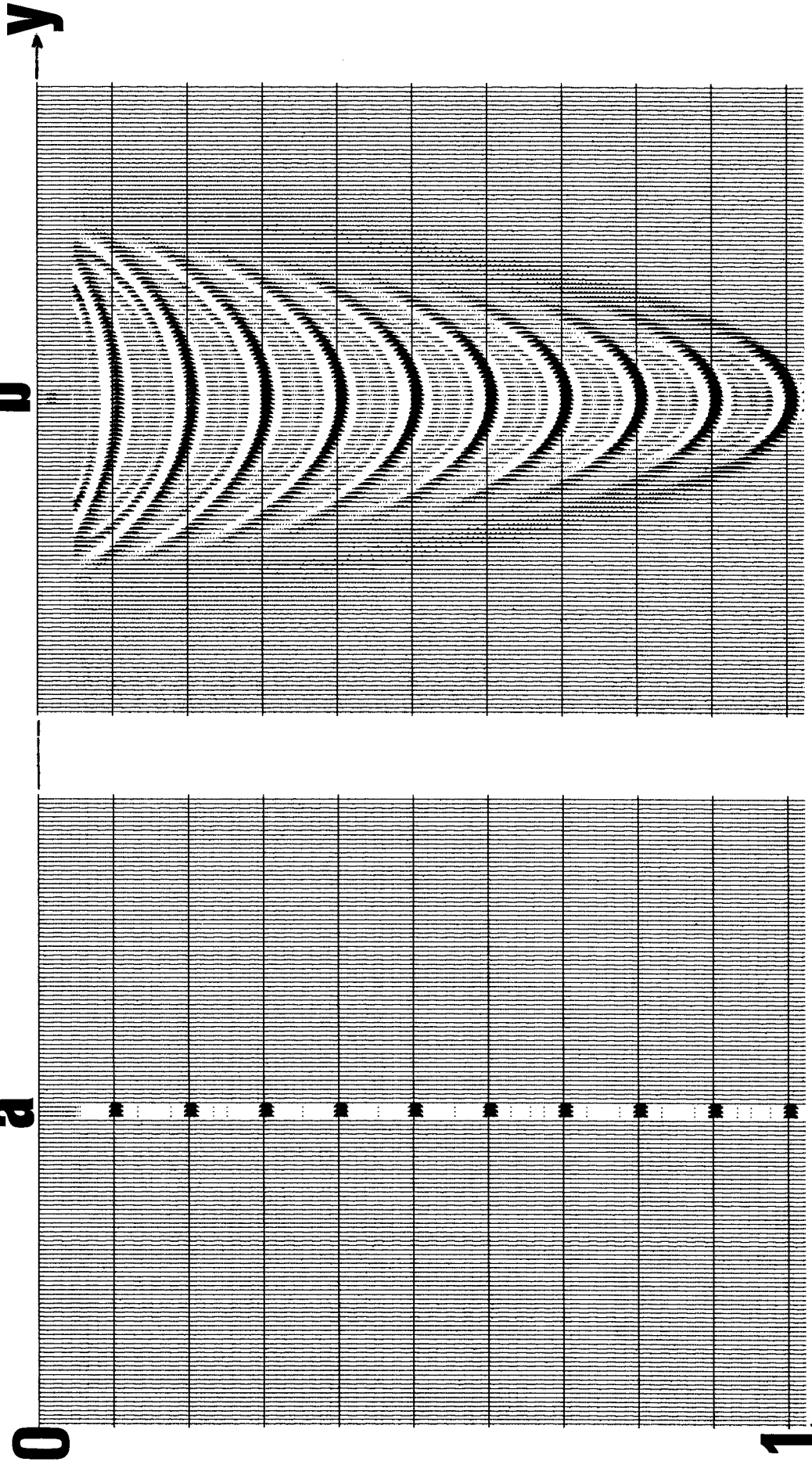


FIG. 2-7. Impulse response of the post-NMO partial migration operator. If (a) is considered to be a common offset section with h = 400 m, (b) is the mapping to zero offset. Note the similarity of the behavior to the response of the pre-NMO operator shown in Figure 2-6 and the response generated by the inverse Fourier transformation of the transfer function of Dev(Y,H) shown in Figure 2-1b.

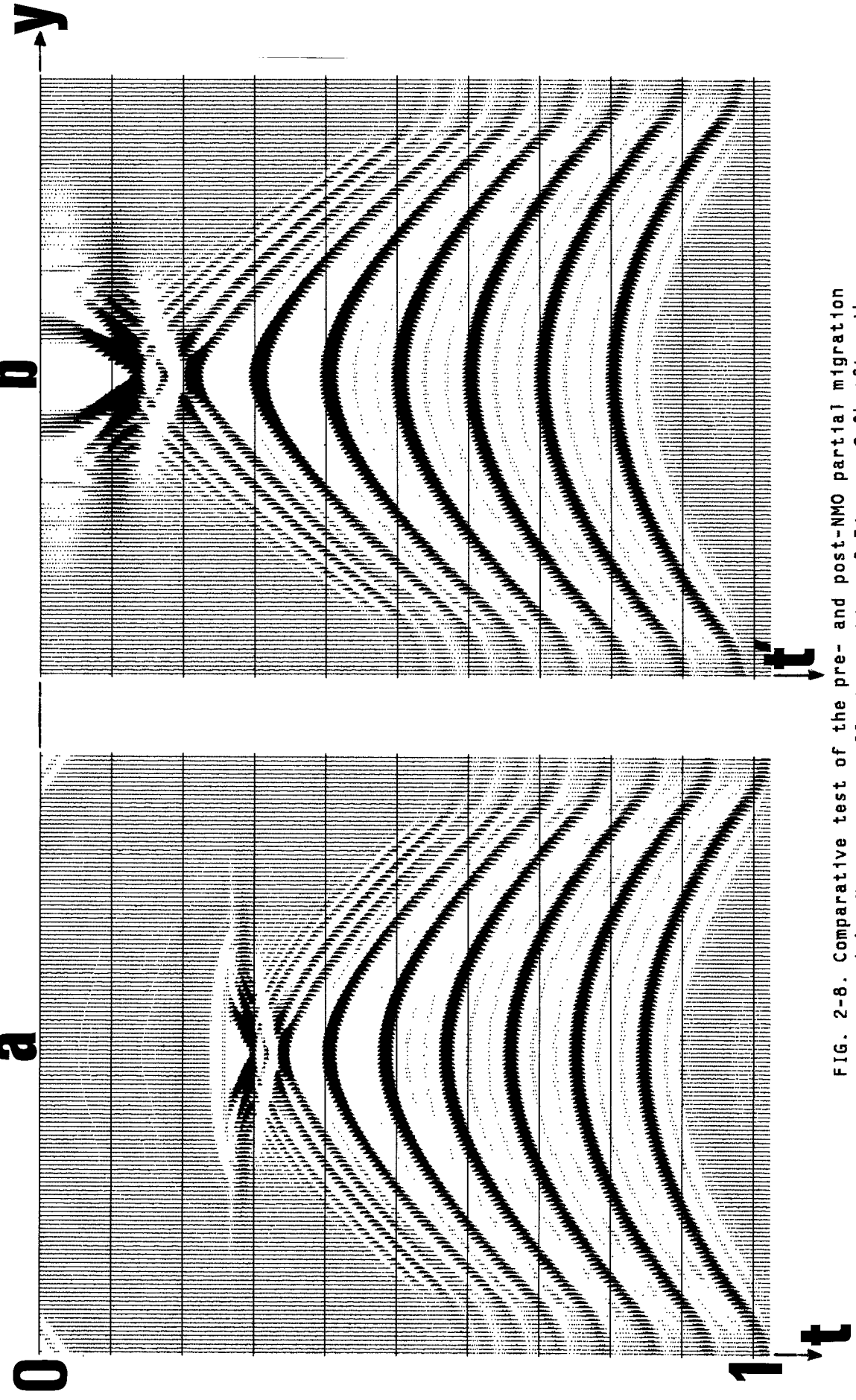


FIG. 2-8. Comparative test of the pre- and post-NMO partial migration procedures. (a) The common offset section of Figure. 2-3b after the pre-NMO partial migration; and (b) the moveout-corrected version of (a). Compare with Figure 2-9b and the zero offset section shown in Figure 2-3a.

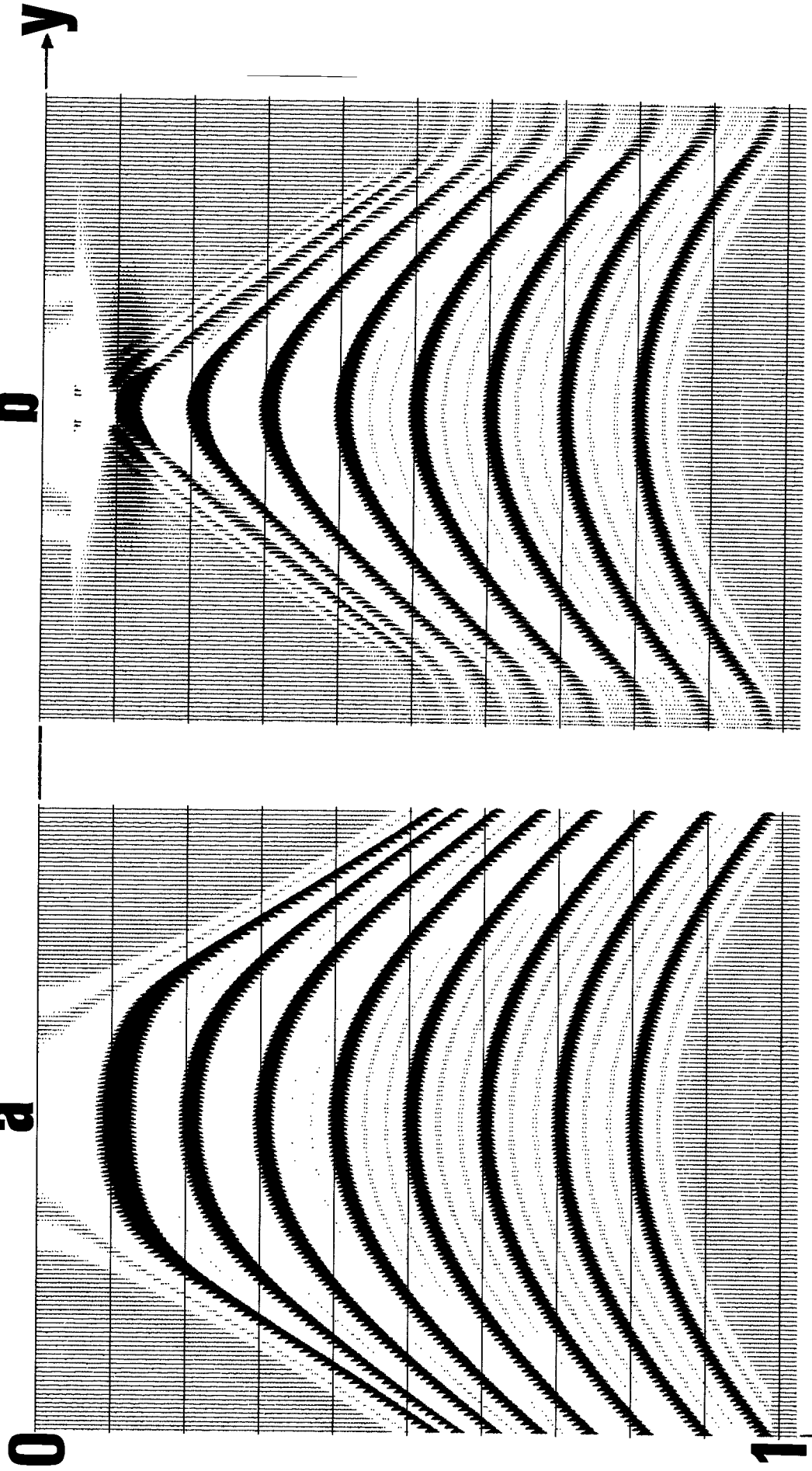


FIG. 2-9. (a) Moveout-corrected common offset section of Figure 2-3b. The low-frequency appearance of the top event is due to stretching during moveout correction. (b) Partial migration of (a) using the post-NMO operator. Note that performance is better than with the pre-NMO operator as shown in Figure 2-8b, particularly in the shallow portion. Compare with the zero-offset section shown in Figure 2-3a. Dispersion near the top arises due to the insufficient accuracy of the differential equation for very large offset angles.

performance of our equations is to migrate the outputs of Figures 2-8b and 2-9b, and compare the results with the migrated zero-offset section. Figure 2-10 clearly shows the effect of the operator on the performance of migration. Here we used the 15-degree migration scheme for the sake of convenience. Certainly other schemes, such as the 45-degree or the frequency domain algorithms, can be used for better imaging. However, no migration algorithm can possibly collapse the energy at or near $k_y = 0$ in Figure 2-10b.

How sensitive is the operator to velocity variation and offset value? Figure 2-11 shows that a 20% deviation from the true medium velocity did not make any significant difference. However, a 25% change in offset value did have an effect on the output, as shown in Figure 2-12.

We tested the pre-stack partial migration equation (2-31) on the variable velocity v(z) model shown in Figure 2-13. Common offset sections with h = 0 and h = 400 m are shown in Figure 2-14. The zero-offset mapping using the post-NMO operator is shown in Figure 2-15. Again, subsequent migration (Figure 2-16) is more effective on the section that was partially migrated.

Let us now simulate the entire sequence of seismic data processing by considering a 6-fold point scatterer model. Offset values are h = 0-1000 m with an increment of 200 m. The zero and the farthest offset sections are shown in Figure 2-17 for comparison. Figure 2-18a shows every twelfth CMP gather starting from the left and going to the center of the model. First let us follow the conventional route. Moveout-corrected CMP gathers are shown in Figure 2-18b. We can clearly see the effects of steep dip and large offsets on the NMO correction. The CMP gather from the central trace where dip is zero is perfectly flattened. Moving up to the left, however, we see the over-corrected gathers [ Levin effect (Doherty, 1975)]. The resulting CMP stack is shown in Figure 2-19a. Ideally, we would like to have a zero-offset section like the one shown in Figure 2-17a. Let us now include the pre-stack partial migration process in the conventional sequence. Applying the post-NMO operator on moveout-corrected common offset sections we have the CMP

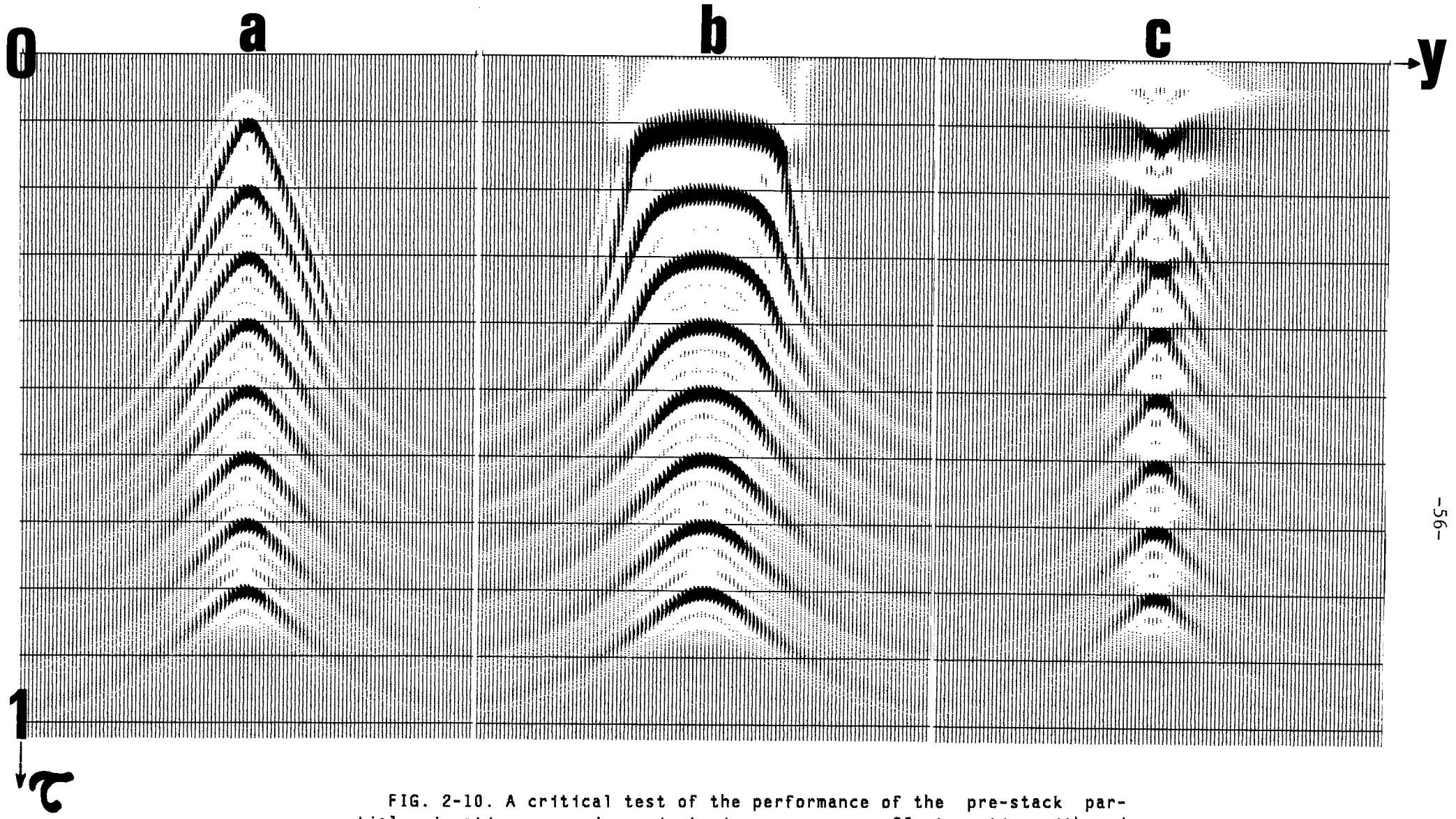


FIG. 2-10. A critical test of the performance of the pre-stack partial migration procedure is to image a common offset section with and without applying this procedure. (a) is the migrated zero-offset section shown in Figure 2-3a; (b) is the migrated non-zero offset section shown in Figure 2-3b, and (c) is the migrated version of the partially migrated non-zero offset section shown in Figure 2-9b. Even though the 15-degree finite difference algorithm was used for migration, no migration scheme can collapse the dominant zero spatial frequency as seen in (b). Note the better imaging obtained by the partially migrated section (c). Under-migration of very high dips in all three cases is due to the 15-degree accuracy.

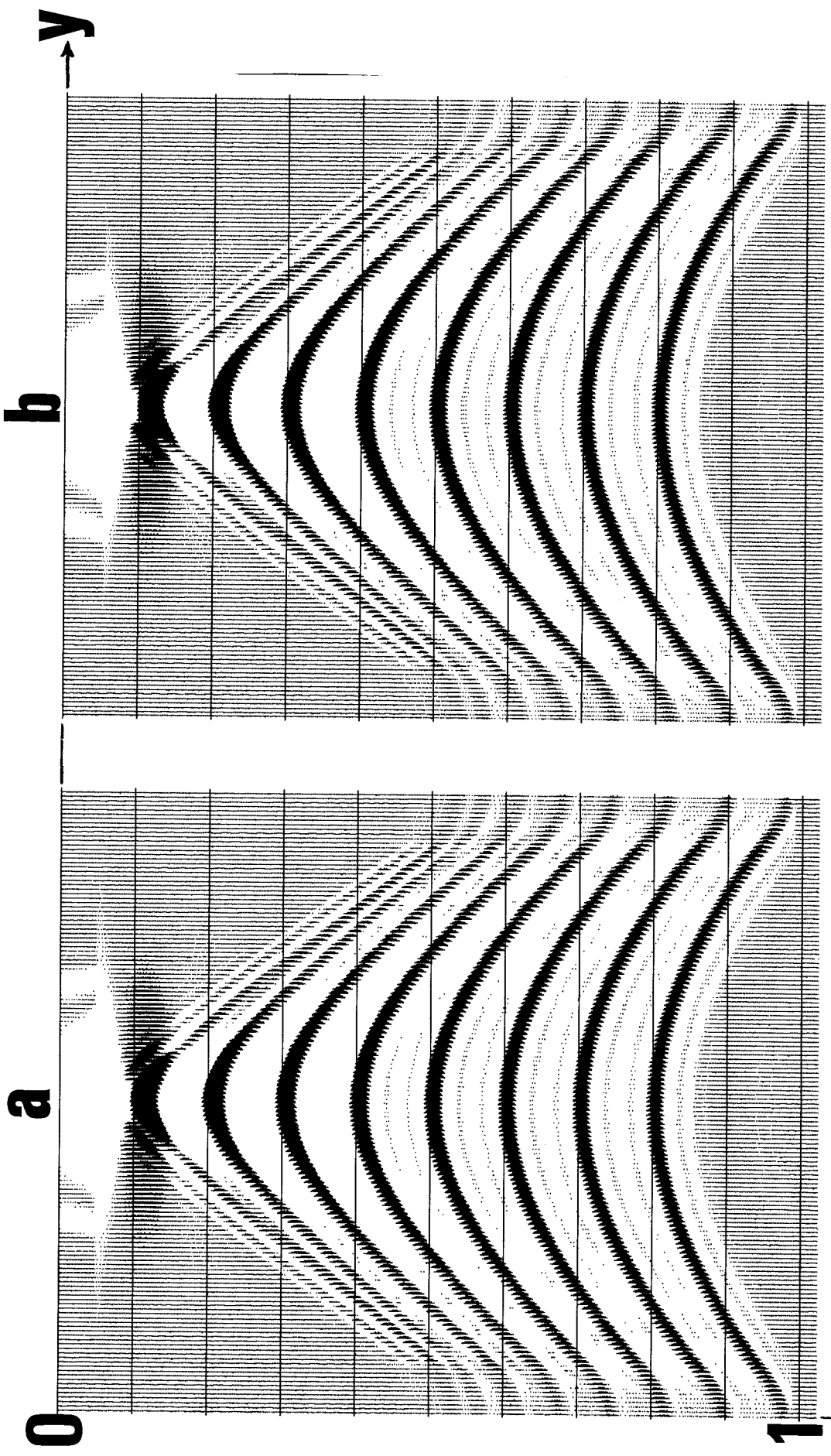


FIG. 2-11. Sensitivity of the partial migration operator to variation in velocity. The true velocity of the medium is 3000 m/sec. Figure 2-9a after partial migration with (a) v = 2400 m/sec, and (b) v = 3600 m/sec. Comparison with Figure 2-9c, which is the partial migration with the correct velocity, clearly indicates that the process is quite robust, i.e. insensitive to significant variations in velocity. This is a desirable property for such a procedure since velocity estimation is usually not completely accurate.

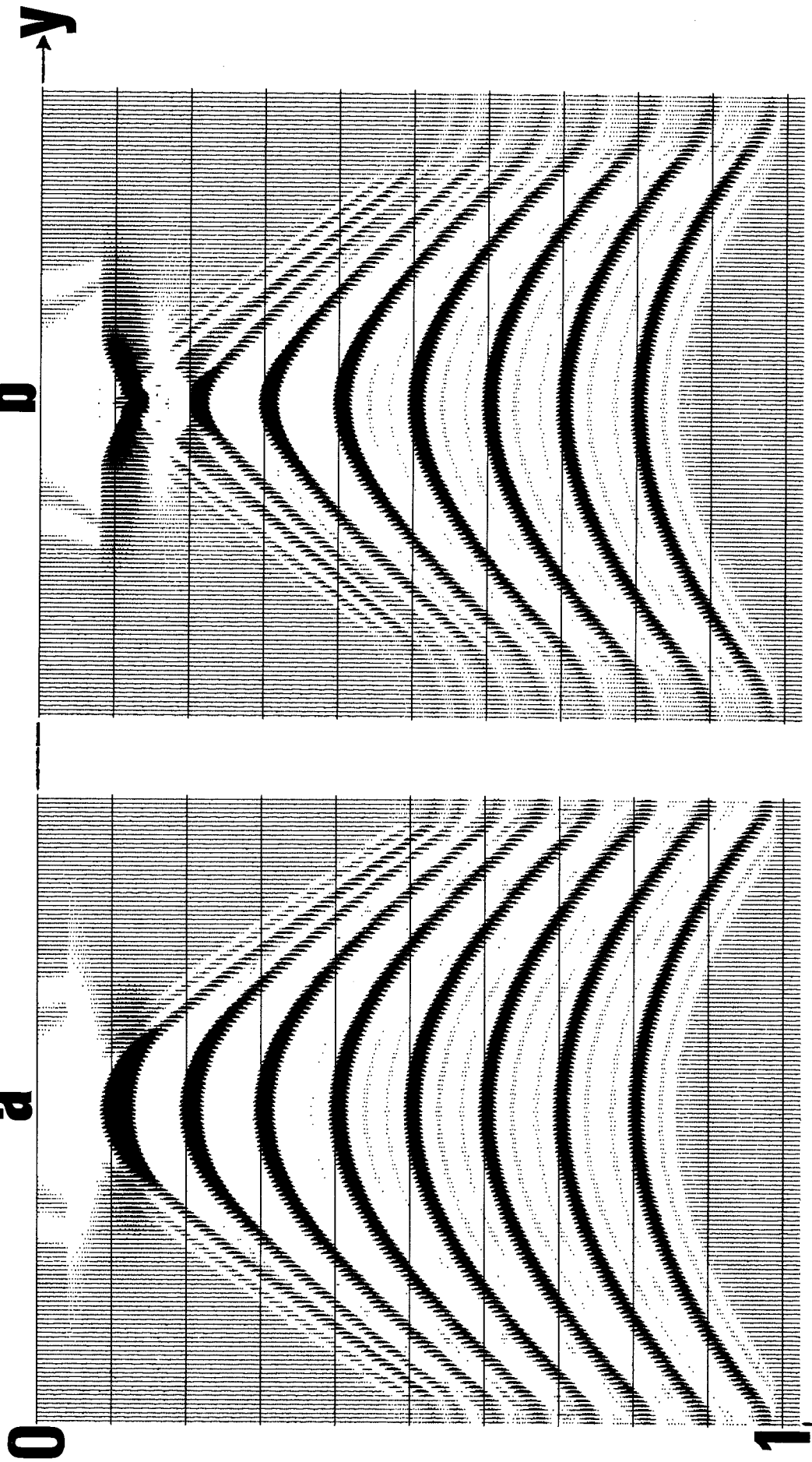


FIG. 2-12. Sensitivity of the partial migration operator to offset value. True offset value is h = 400 m. (a) is the partial migration of the moveout-corrected section shown in Figure 2-9a with a smaller offset value (h = 300 m), as is (b), but with a larger offset value (h = 500 m). As we would expect, with a small offset value the section is under-processed, and with a large offset value it is over-processed.

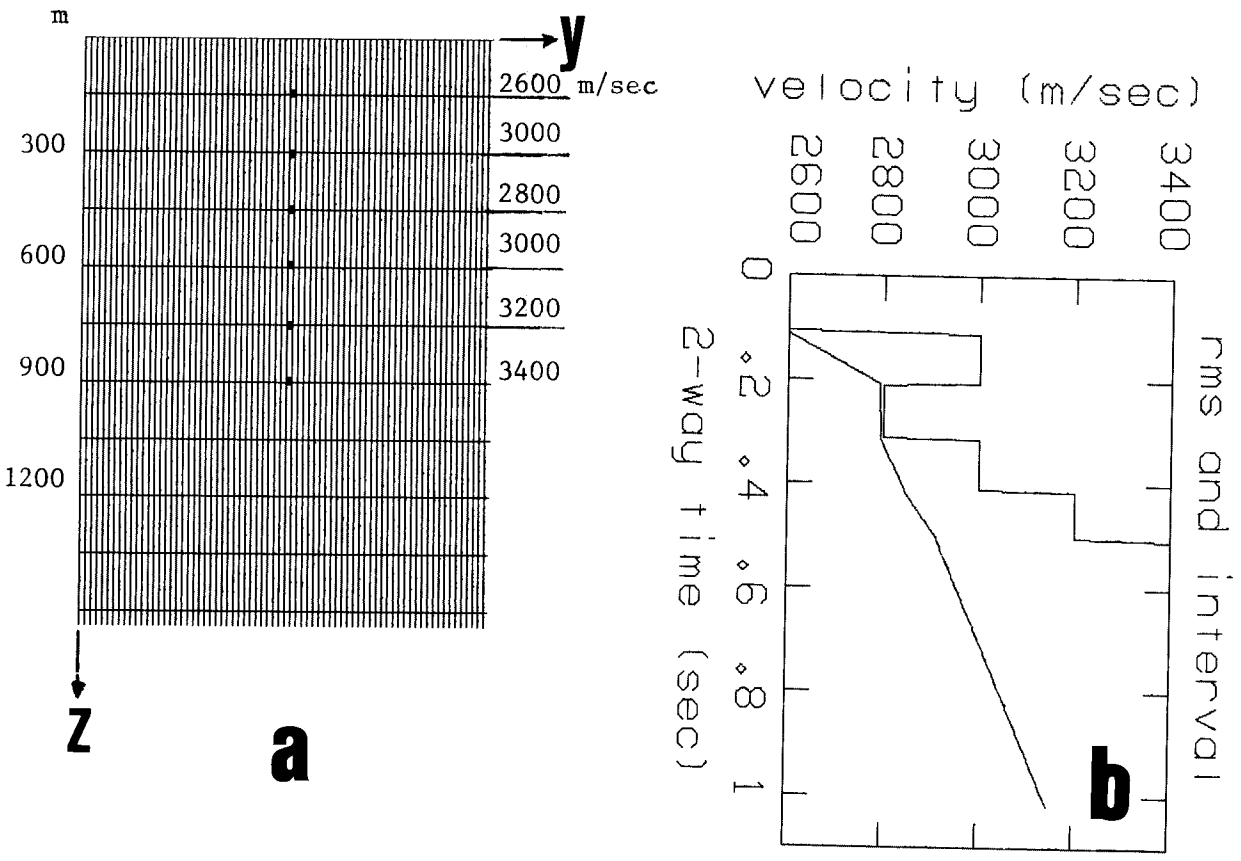


FIG. 2-13. Variable velocity v(z) model. (a) Six point scatterers buried at depths between z = 150-900 m. (b) RMS and interval velocities as a function of zero-offset two-way traveltime.

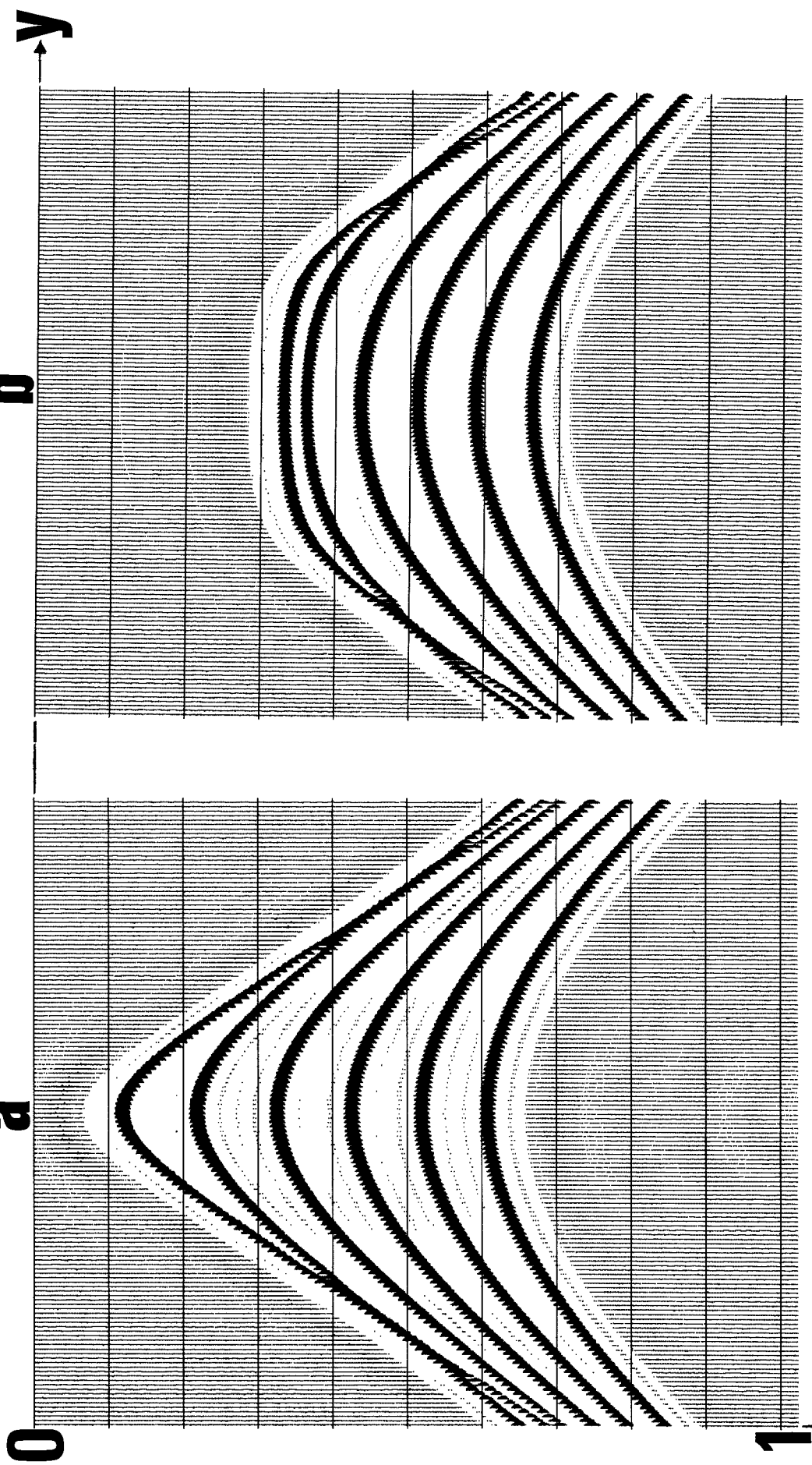


FIG. 2-14. Common offset sections over the variable velocity model shown in Figure 2-13, (a) zero-offset section (h = 0), and (b) common offset section with h = 400 m. Ray path integrals were used to compute the traveltimes. Amplitudes decay as $t^{-1/2}$, and bandwidth is 6,12 - 36,48 Hz. The sampling interval is 4 msec and the midpoint spacing is 12.5 m.

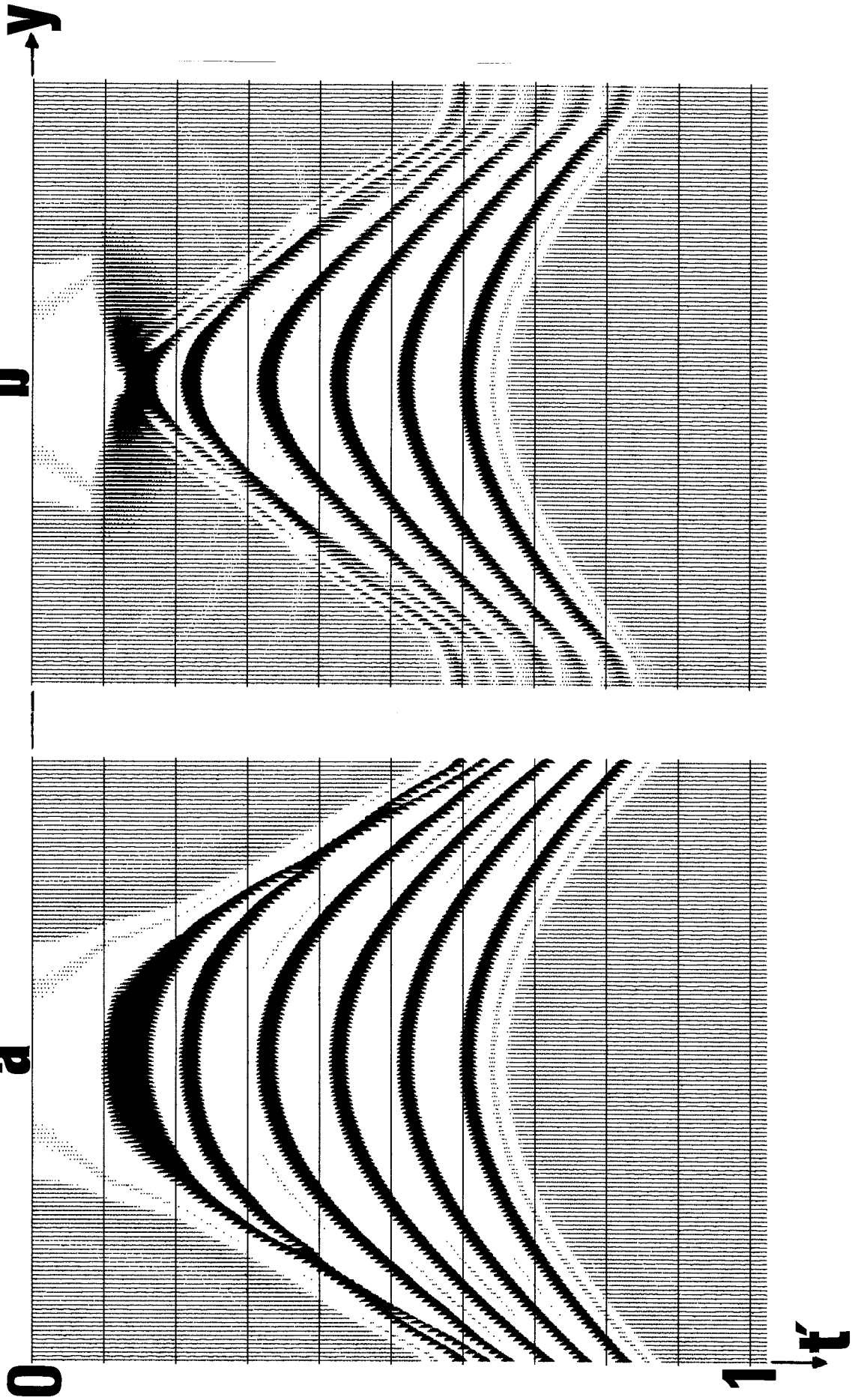


FIG. 2-15. Partial migration (b), applied on the moveout-corrected section (a) of the common offset section shown in Figure 2-14b. Compare with the zero-offset section shown in Figure 2-14a.

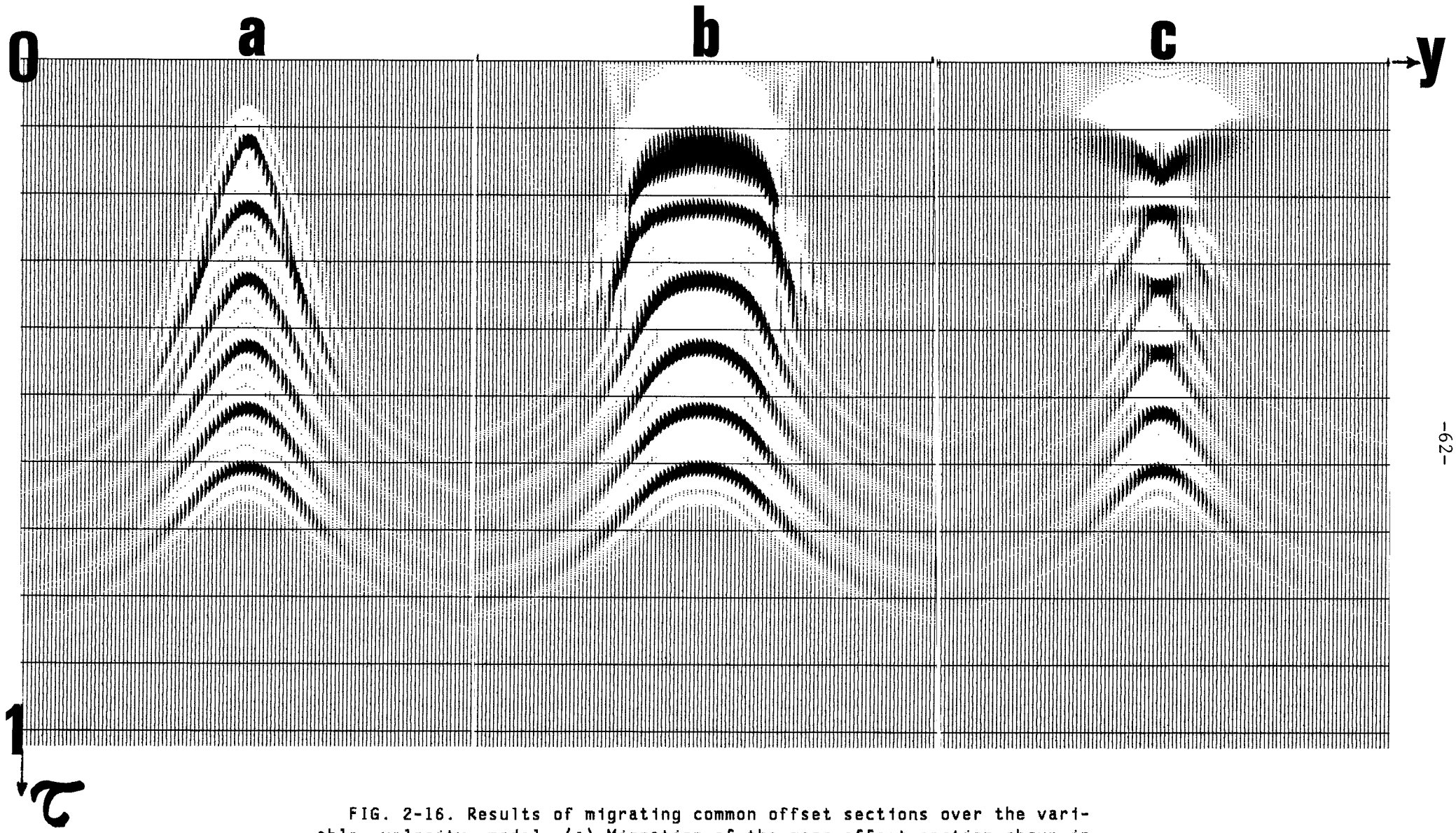


FIG. 2-16. Results of migrating common offset sections over the variable velocity model. (a) Migration of the zero-offset section shown in Figure 2-14a, (b) migration of the moveout-corrected non-zero offset section shown in Figure 2-15a, and (c) migration of the partially migrated section shown in Figure 2-15b. Note the better imaging with the partially migrated section.

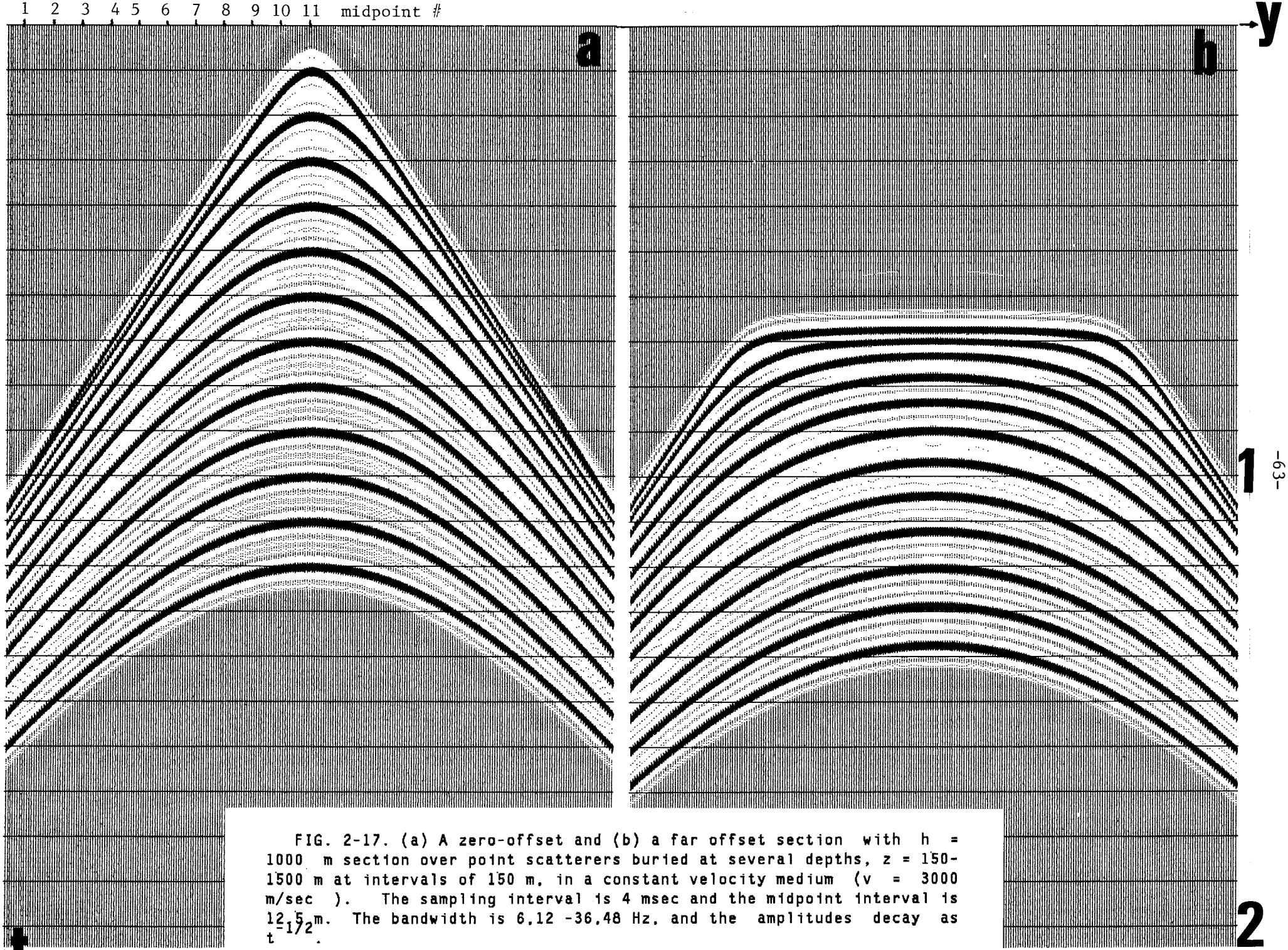


FIG. 2-17. (a) A zero-offset and (b) a far offset section with h = 1000 m section over point scatterers buried at several depths, z = 150-1500 m at intervals of 150 m, in a constant velocity medium (v = 3000 m/sec ). The sampling interval is 4 msec and the midpoint interval is 12.5 m. The bandwidth is 6.12 -36.48 Hz, and the amplitudes decay as $t^{-1/2}$.

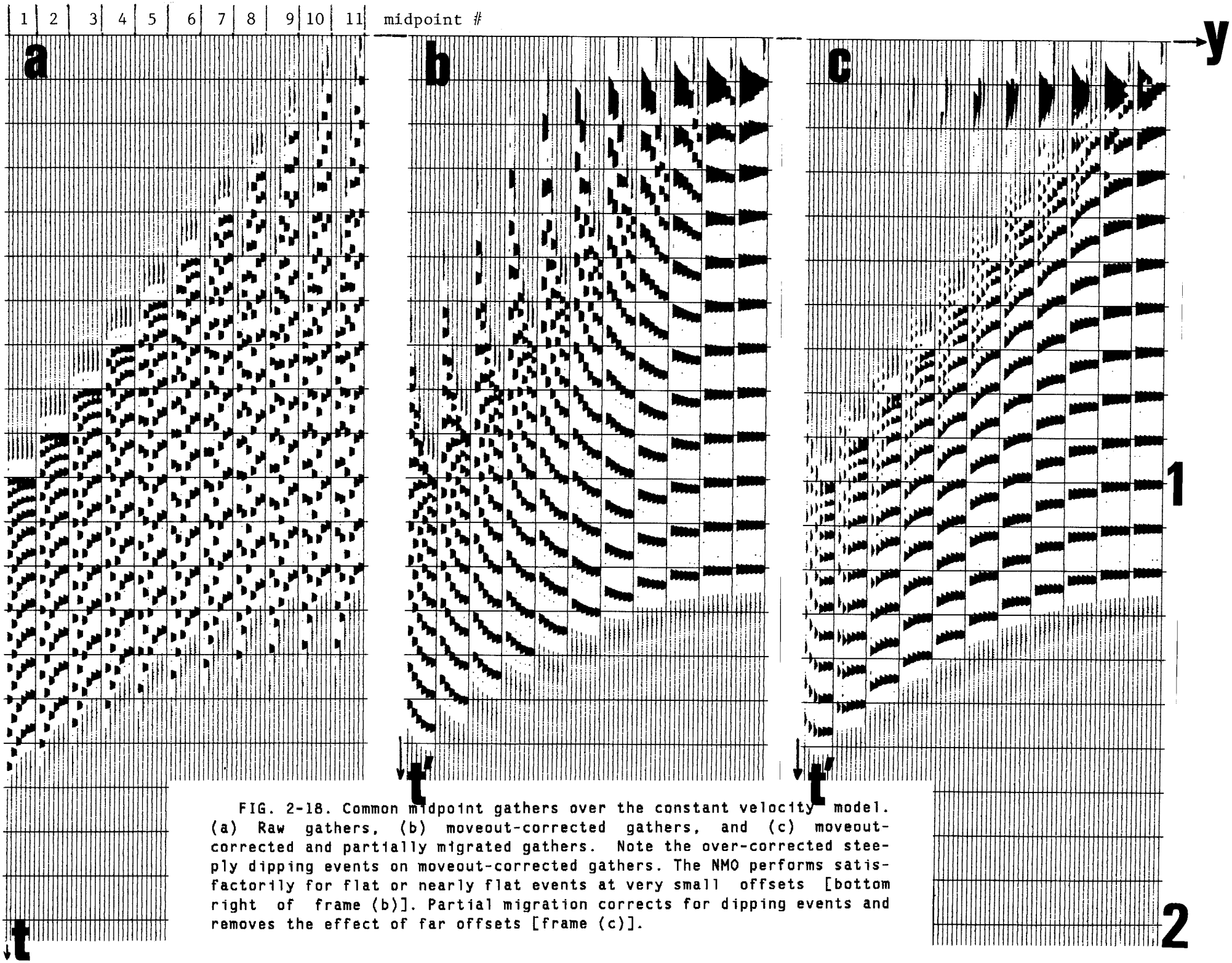


FIG. 2-18. Common midpoint gathers over the constant velocity model. (a) Raw gathers, (b) moveout-corrected gathers, and (c) moveout-corrected and partially migrated gathers. Note the over-corrected steeply dipping events on moveout-corrected gathers. The NMO performs satisfactorily for flat or nearly flat events at very small offsets [bottom right of frame (b)]. Partial migration corrects for dipping events and removes the effect of far offsets [frame (c)].

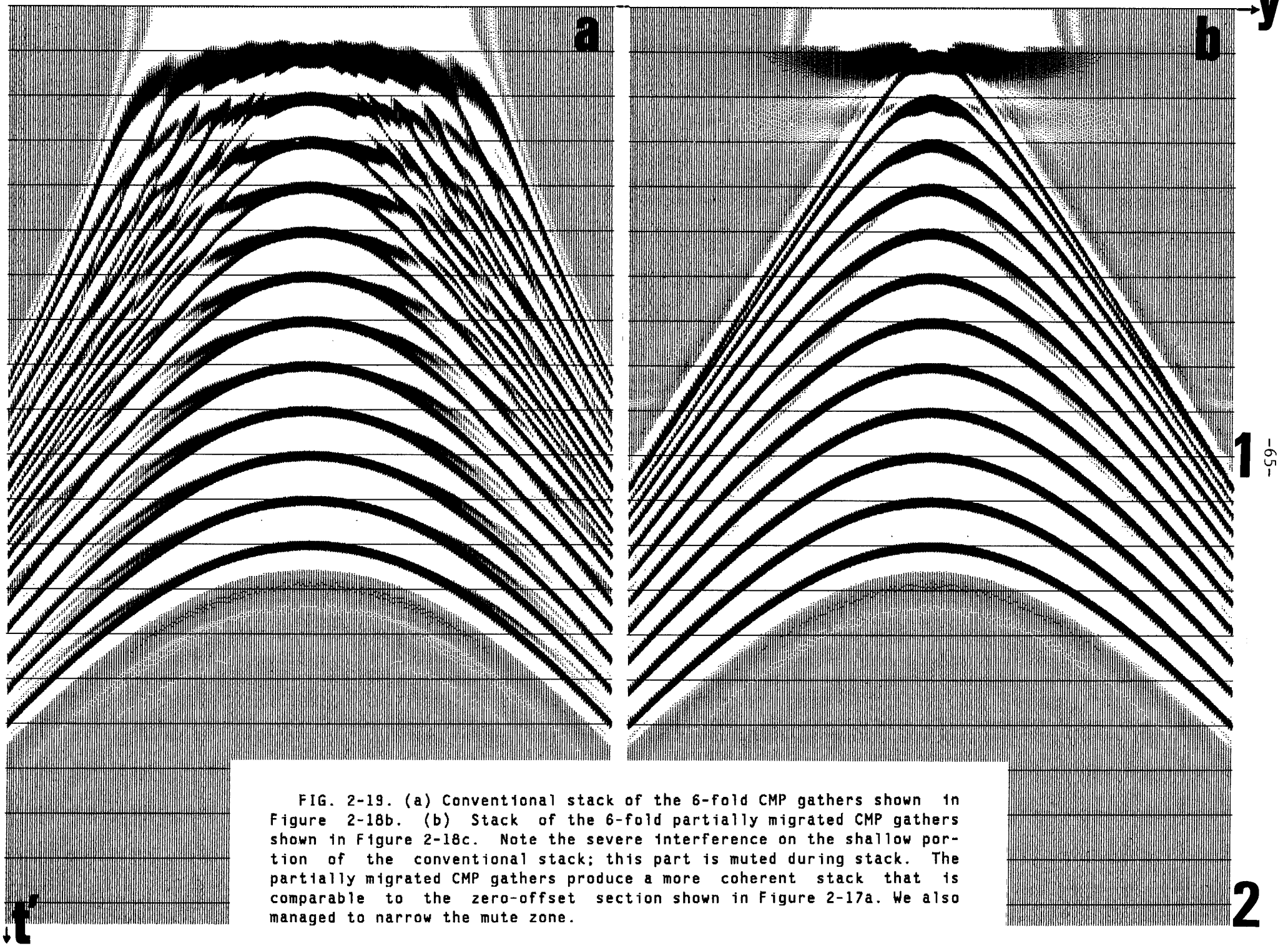


FIG. 2-19. (a) Conventional stack of the 6-fold CMP gathers shown in Figure 2-18b. (b) Stack of the 6-fold partially migrated CMP gathers shown in Figure 2-18c. Note the severe interference on the shallow portion of the conventional stack; this part is muted during stack. The partially migrated CMP gathers produce a more coherent stack that is comparable to the zero-offset section shown in Figure 2-17a. We also managed to narrow the mute zone.

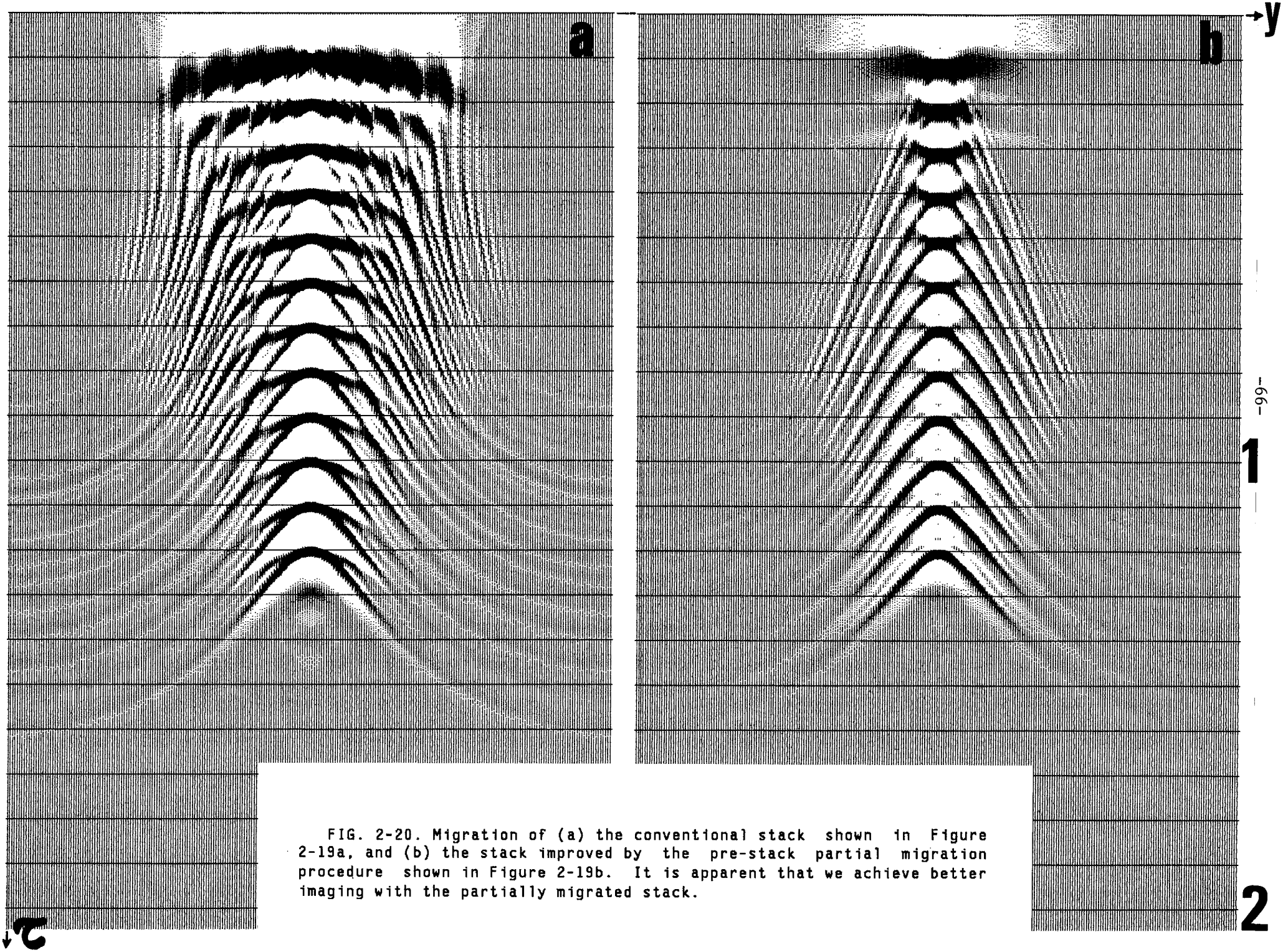


FIG. 2-20. Migration of (a) the conventional stack shown in Figure 2-19a, and (b) the stack improved by the pre-stack partial migration procedure shown in Figure 2-19b. It is apparent that we achieve better imaging with the partially migrated stack.

gathers shown in Figure 2-18c. Notice the considerable improvement in the wide offset and steep dip regions. In the upper part of the CMP gathers we see events that are not corrected properly. This is because these events have dips that are beyond the range of dips our operator can handle. The improved CMP stack is shown in Figure 2-19b. The usual practice is that the top portion of the stack is muted. By improving the CMP stack we manage to considerably narrow the mute zone. Doing so, we are able to recover primary energy under the interference zone shown in Figure 2-19a. Migrations of the CMP stacks with and without the post-NMO partial migration are shown in Figure 2-20 . Better imaging is achieved with the pre-stack partial migration.

In summary, we tested the pre-stack partial migration process using models of point scatterers. Results indicate that this process results in a considerable improvement over the conventional stack. The process is quite robust, i.e. insensitive to any significant velocity variations. The mute zone is narrowed and better imaging is achieved by post-stack migration.

## *2-4 Field Data Example*

A field dataset provided by Digicon, Inc. from the Gulf of Mexico was processed using the pre-stack partial migration equation. The data is 48-fold with offsets varying between 1037-12740 ft. The processing sample rate is 4 msec, and the total record length is 5 sec. The number of midpoints is 282, with an interval of 83 ft.

Following is the processing sequence:

(1) At every sixth midpoint, velocity estimation was done by the semblance technique, which is widely used in exploration seismology at present. An example is shown in Figure 2-21a . The velocity function was chosen which stacked flat or near flat events best, free of any dip effects (Figure 2-21b).

(2) Using this velocity function, CMP gathers were moveout corrected, simultaneously stacking every four adjacent offsets. Thus we reduced the

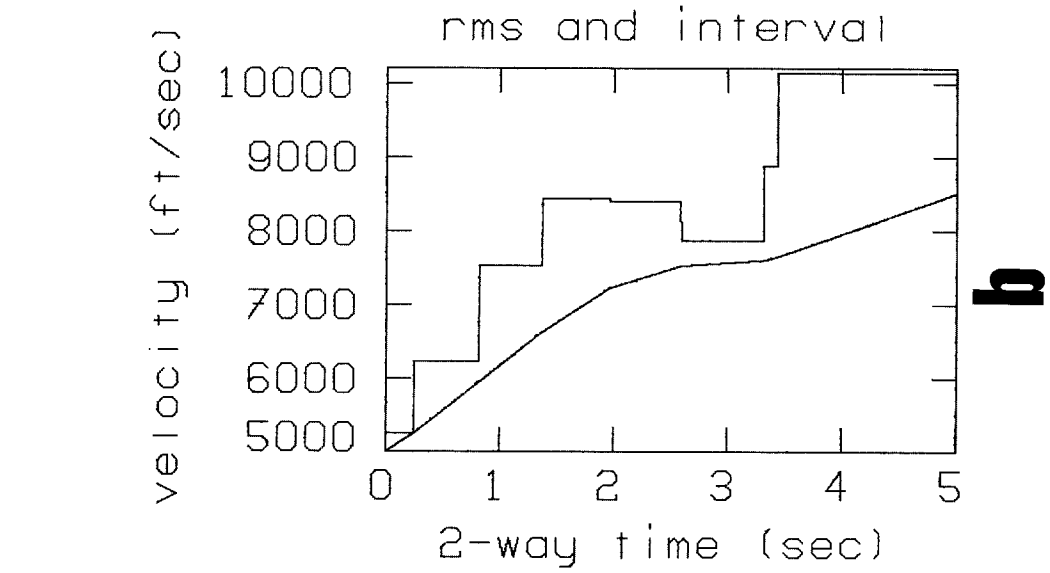


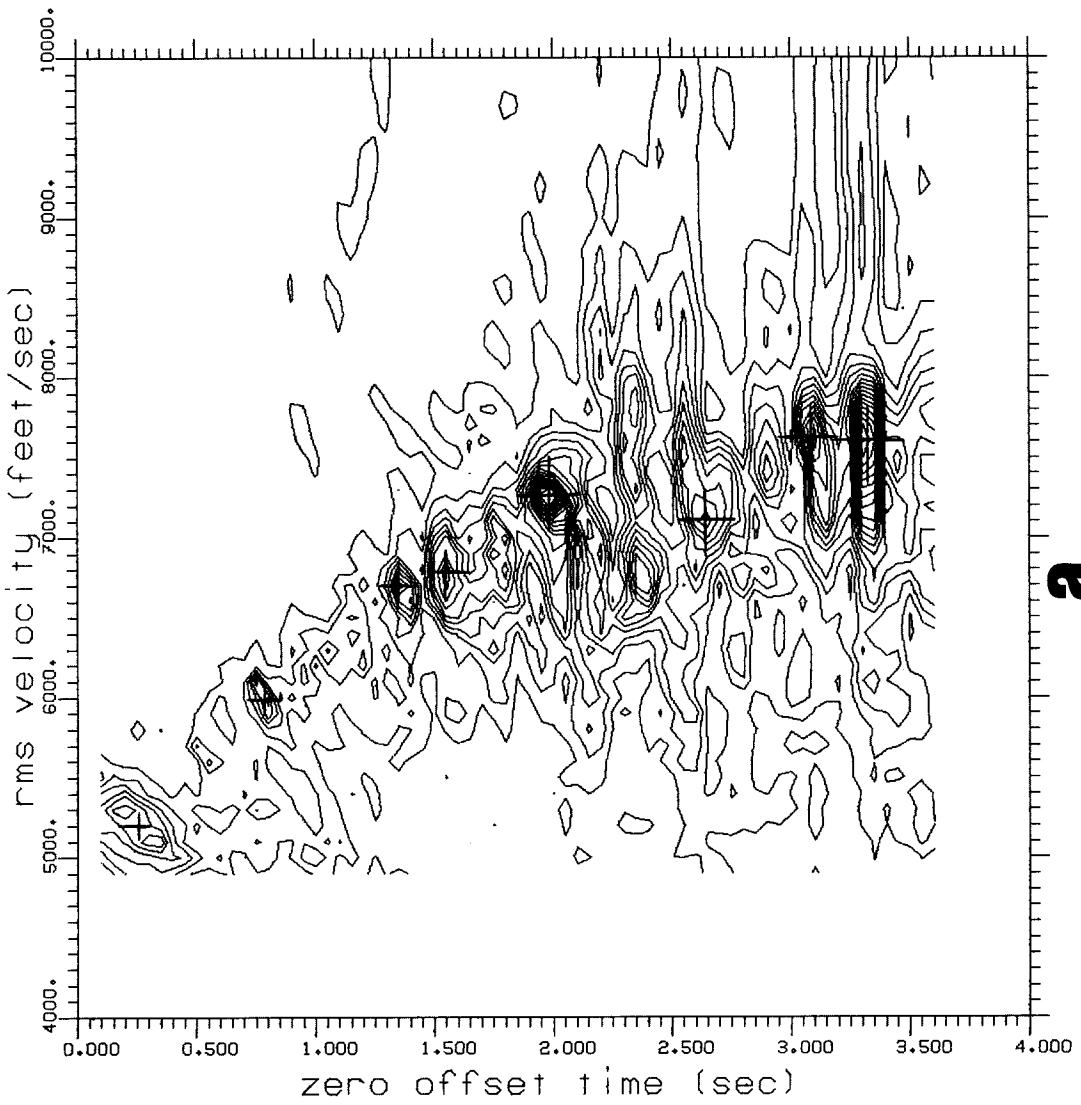


FIG. 2-21. (a) Velocity analysis on the field data example used in testing the pre-stack partial migration procedure. The semblance function was computed using several velocity values plotted against two-way zero-offset traveltime. This particular semblance map is for the mid-point number 37 on the common offset section shown in Figure 2-22a. (b) The velocity curve used in processing the field data was chosen as an optimal function from several semblance maps. It stacks flat or nearly flat events best.

size of the data by creating substacks while enhancing the signal-to-noise ratio. Considerable subsequent computational effort was also saved in this way. Certainly, substacks are allowable for only a narrow range of offset values. To give an idea as to the nature of the data dealt with, Figure 2-22 shows two moveout-corrected substacks (common offset sections). Notice that the dipping events related to steep fault planes are well pronounced on the far offset section while on the near offset section they are hardly evident.

(3) Figure 2-23 shows the conventional stack of moveout-corrected CMP gathers. An average muting function was chosen from several CMP gathers. Notice the degradation of the steeply dipping events that are actually present in wide-offset sections. This clearly demonstrates the fact that, on real data, conventional stack handles wide offsets inadequately. Figure 2-24 shows some of the moveout-corrected CMP gathers. We see that dipping events are overcorrected, thus resulting in poor coherency in stack.

(4) The moveout-corrected common offset sections were partially migrated using Equation (2-31), in which $\hat{H}$ was adjusted for a regional dip of 45 degrees. The effect of this process is seen on the CMP gathers shown in Figure 2-25. Note that flat events are left as they are, but on dipping events the offset effect was removed.

(5) Subsequent stacking (Figure 2-26) is superior to the conventional stack shown in Figure 2-23. Dipping events present in the far-offset data are well preserved.

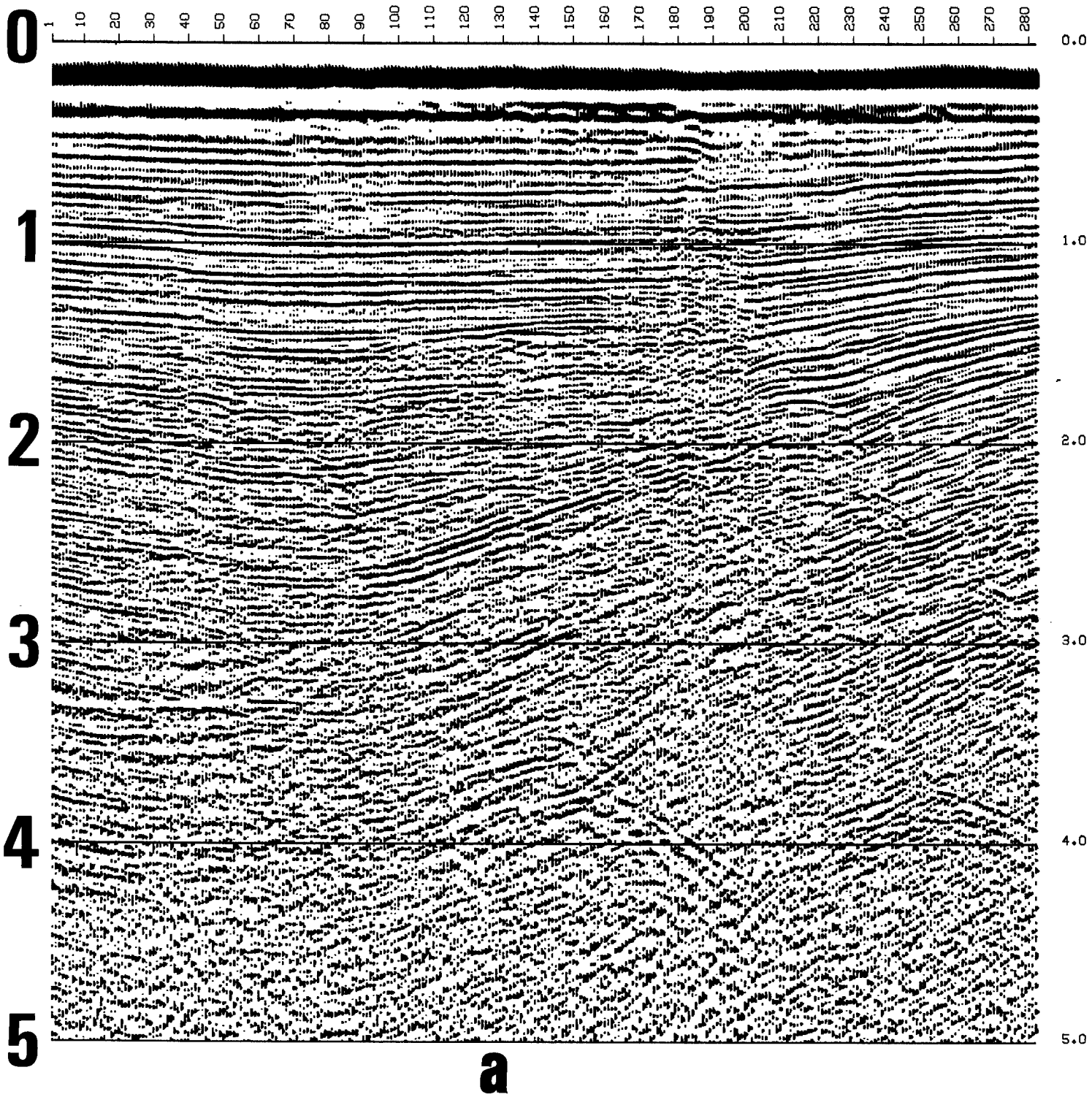


FIG. 2-22. A near (a) and a far (b) common offset section of the Gulf data. Note that the steeply dipping events related to growth fault planes are quite evident in the far offset section. They are hardly visible, however, in the near offset section.

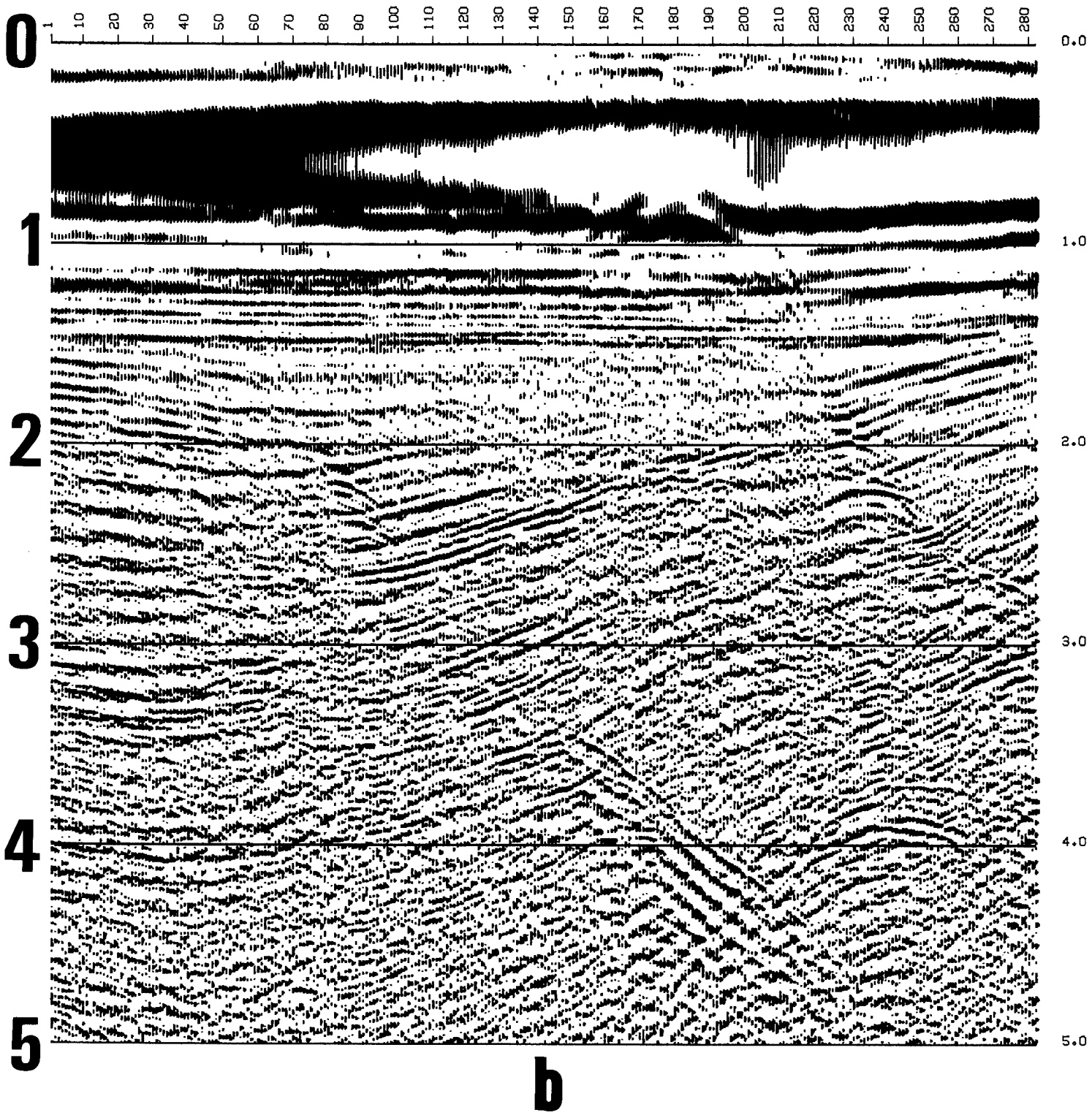


FIG. 2-22. continued.

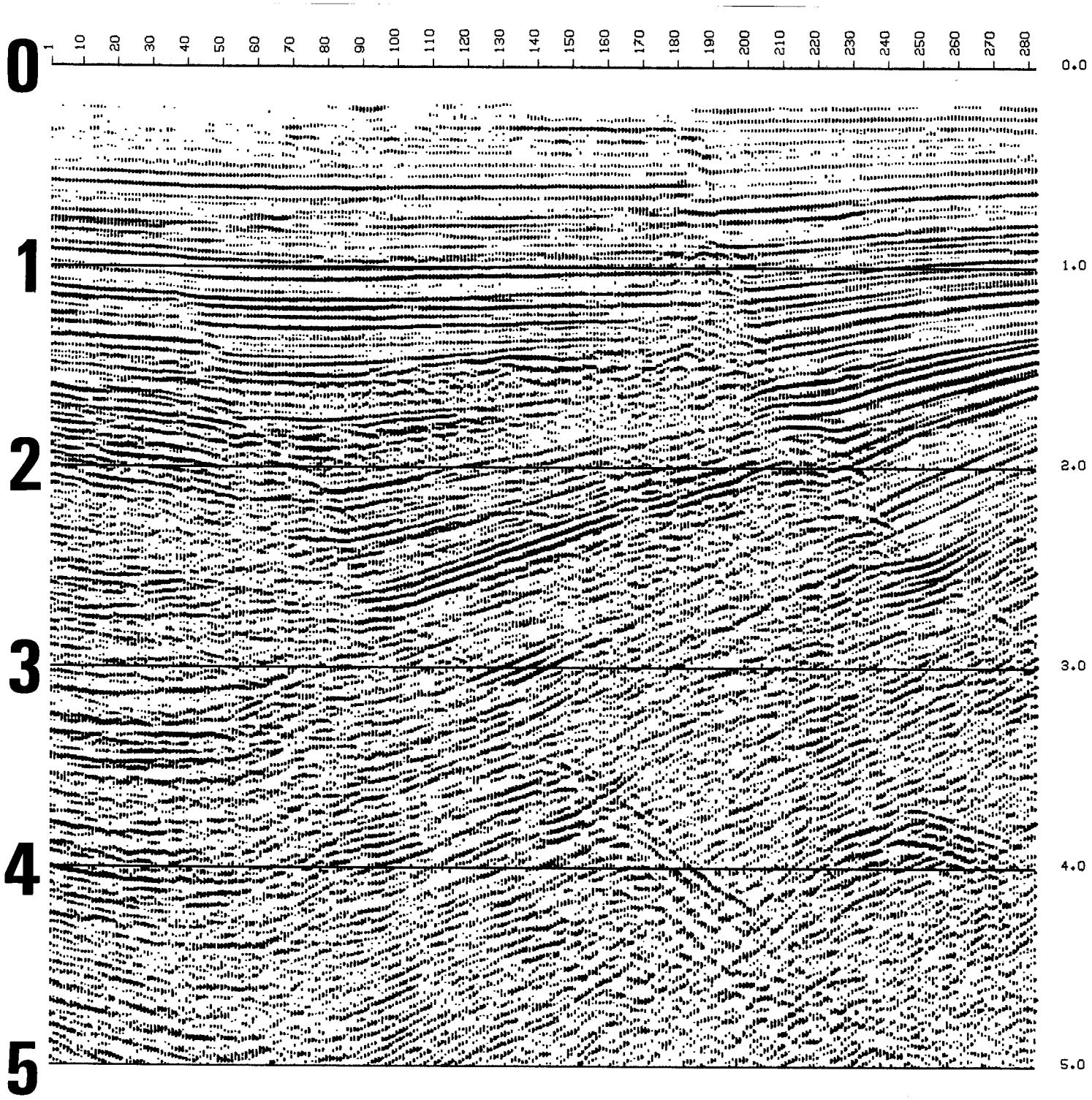


FIG. 2-23. Conventional processing of the Gulf data: moveout correction + stack + a band-pass with cutoff frequencies 6,12 - 48,72 Hz. Note that the steeply dipping events are not stacked properly, even though they are present in most of the common offset sections individually, such as the one in Figure 2-22b.

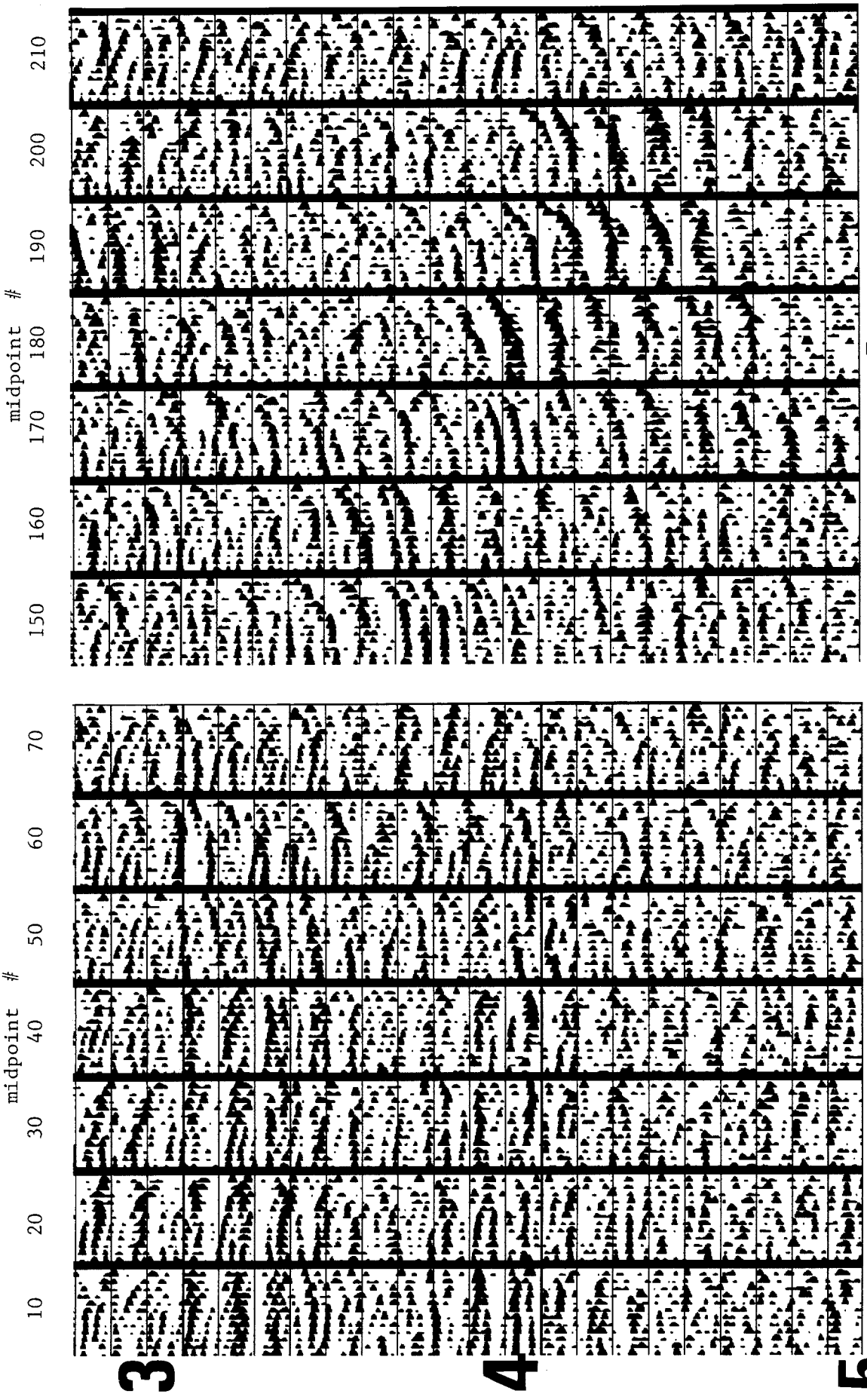


FIG. 2-24. Moveout-corrected CMP gathers from the Gulf data. Flat events (a) have been corrected properly, but dipping events (b) are obviously over-corrected.

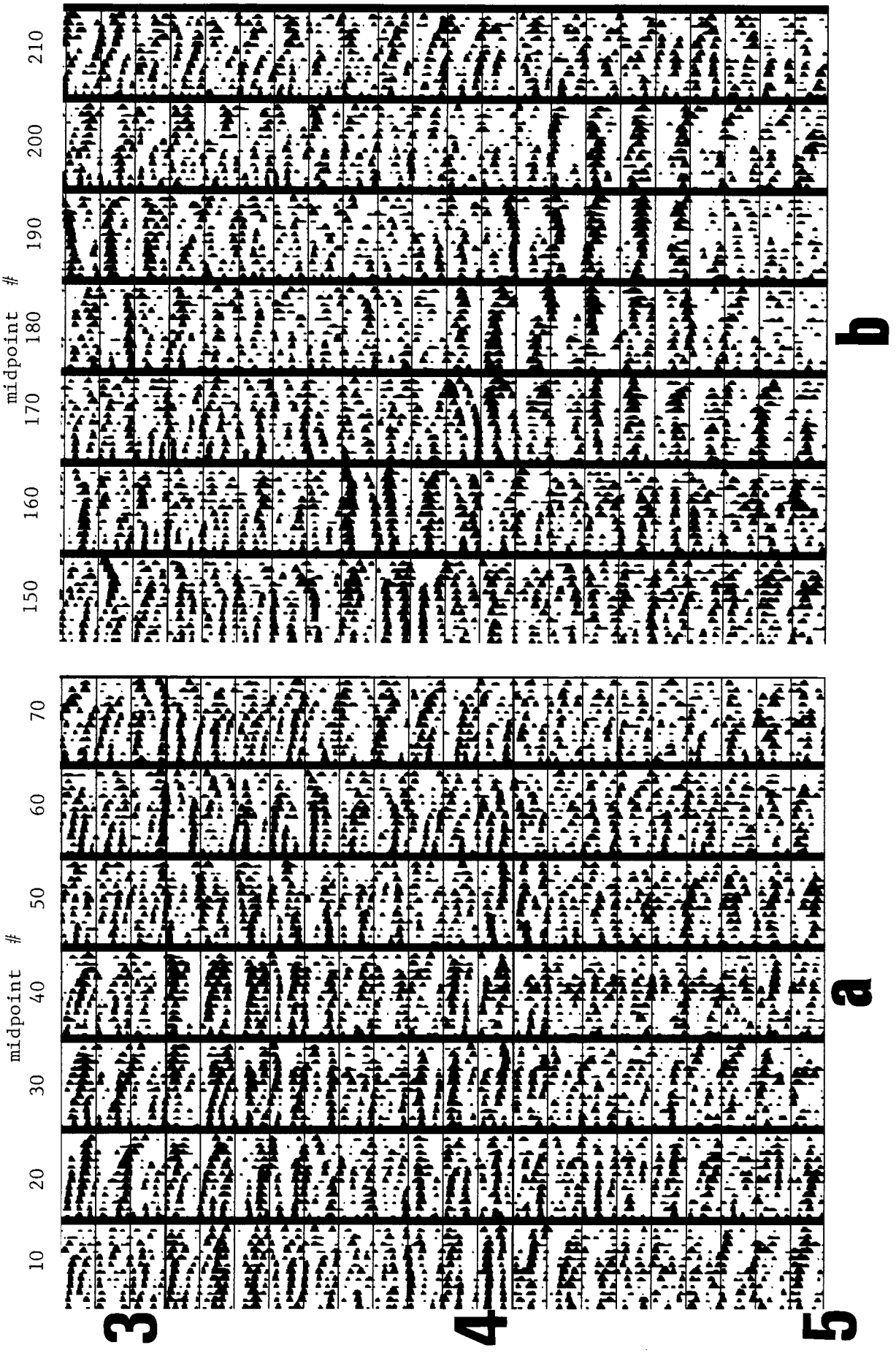


FIG. 2-25. Moveout-corrected CMP gathers after partial migration. (a) Flat events were left as they are, but (b) dipping events were corrected so that they stack coherently.

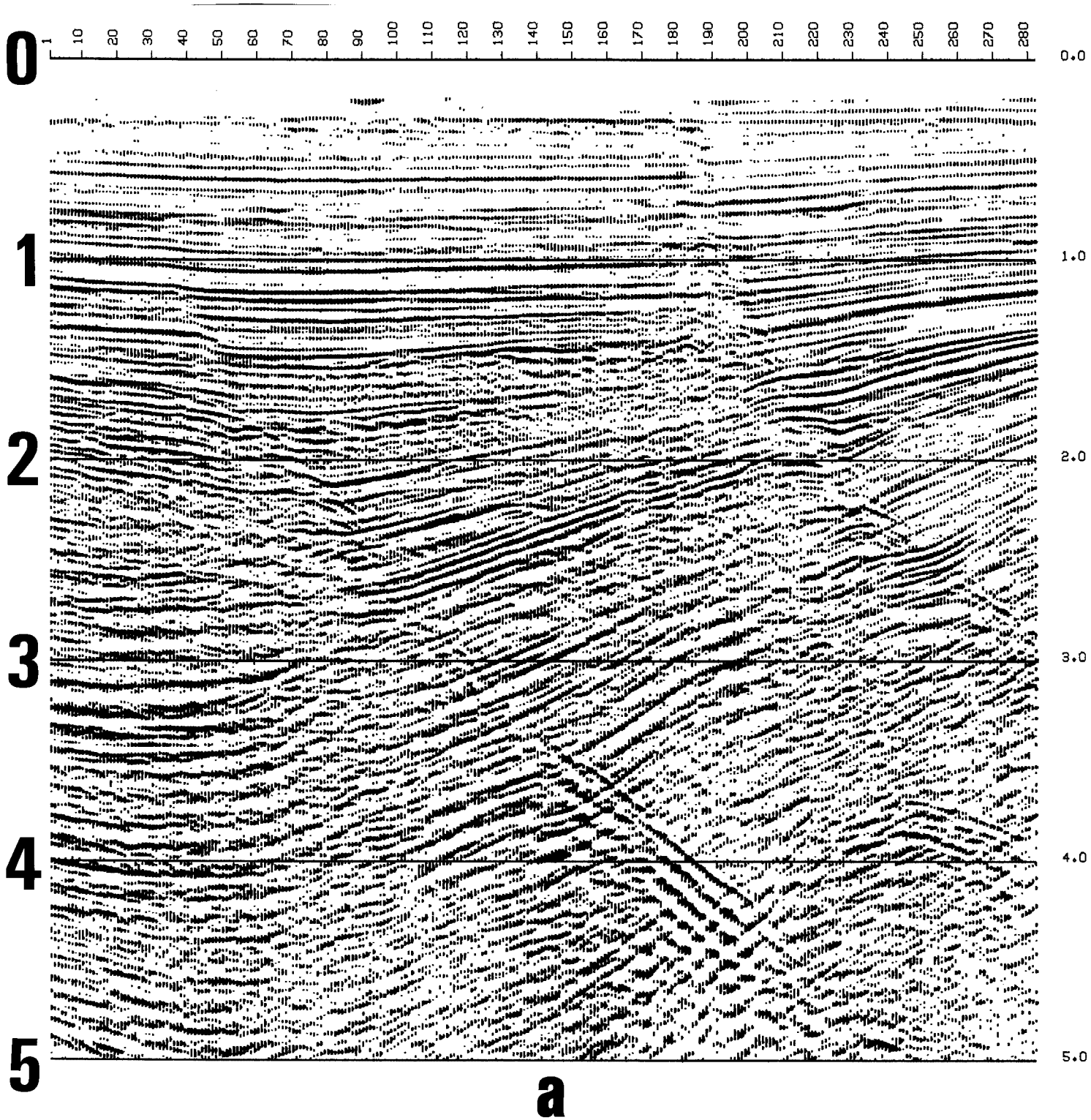


FIG. 2-26. Stack of the partially migrated CMP gathers. Comparison with the conventional stack shown in Figure 2-23 indicates the considerable improvement of dipping events. (a) NMO + partial migration + stack. (b) Band-pass applied on (a) with cutoff frequencies 6,12 - 48,72 Hz.

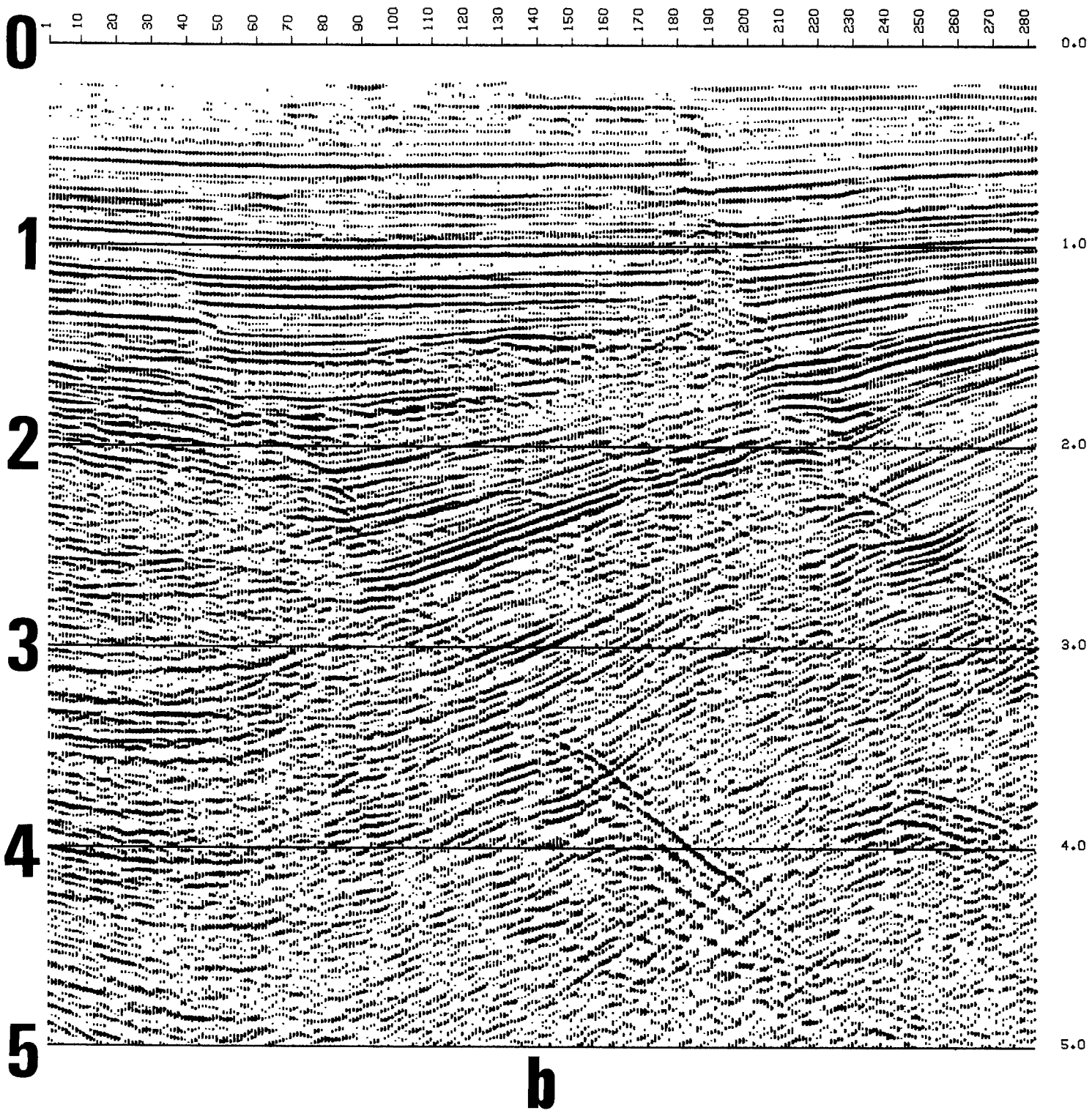


FIG. 2-26. continued.